REMUNOM
ISSN 2178-6925

Received: 13/04/2026 - **Accepted:** 27/05/2026
Vol: 13.11
DOI: 10.66104/y1333s58
Pages: 1-50

ADSORPTION OF Zn^{2+} BY FUNCTIONALIZED RICE HUSKS IN A FIXED-BED COLUMN: DESIGN PARAMETERS AND KINETIC MODELING

Thamires Mirian Zanelatto[a], Plínio Ribeiro Fajardo Campos[a], Veronice Slusarski-Santana[a], Leila Denise Fiorentin-Ferrari[a], Edson Antonio da Silva[a], Fernando Palú[a]

[a] Postgraduate Program in Chemical Engineering, State University of Western Paraná, Toledo, PR, Brazil.

GRAPHICAL ABSTRACT

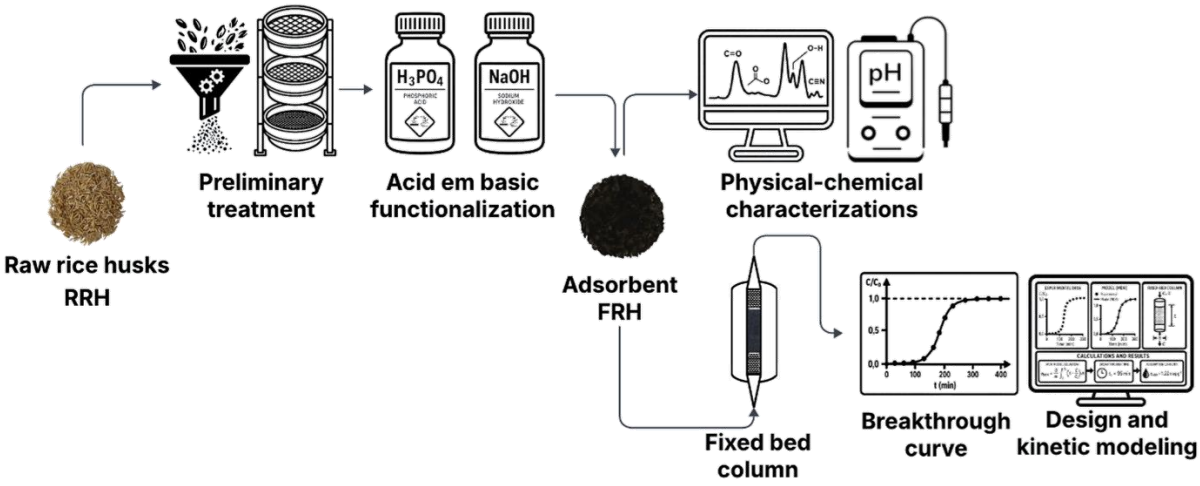

Keywords:

Wastewater treatment
Heavy metals
Agro-industrial waste
Continuous system

ABSTRACT

In this study, rice husks functionalized with H_3PO_4 and NaOH (FRH) were evaluated as an adsorbent

for the removal of Zn^{2+} ions in a continuous system. Breakthrough curves were obtained at different bed heights (5, 10, and 15 cm, at 5 meq L^{-1}) and initial metal concentrations (3, 4, and 5 meq L^{-1}, at 15 cm), from which column sizing and kinetic modeling were performed. As a result, increasing the metal load in the system's feed solution reduced the bed's saturation time ($t_{s,u}$), while increasing the adsorbent height prolonged this parameter's value. Efficiencies of 69.44% and 68.87% were obtained for the 15 cm at 3 meq L^{-1} and 10 cm at 5 meq L^{-1} configurations, respectively. The modified dose-response model (MDR) provided the best fit for most of the evaluated conditions, yielding a q_{MDR} of 1.22 meq g^{-1} for the 5 cm bed at 5 meq L^{-1}. Surface characterization revealed the presence of functional groups responsible for the affinity of FRH toward Zn^{2+} ions, while electrochemical and metal speciation analyses indicated pH 5 as the most favorable condition for conducting the tests. Thus, the FRH adsorbent demonstrated satisfactory performance in the removal of Zn^{2+} under continuous-flow conditions, highlighting not only the use of a low-cost agro-industrial waste as raw material but also for the integration of experimental research, kinetic modeling, and fixed-bed column sizing, aspects essential for obtaining useful parameters for design from the laboratory to industrial applications. Therefore, the material's potential for use in continuous treatment systems for effluents containing heavy metals was demonstrated, contributing to the development of technically viable adsorption technologies applicable on a full-scale basis.

1. INTRODUCTION

The degradation of natural resources is the result of human activities and the unregulated expansion of industrialization across various economic and social sectors (Vareda *et al*., 2019; Adane *et al*., 2021). The improper disposal of industrial waste has generated significant environmental impacts, posing serious risks to public health and potentially causing lasting damage to ecosystems (Kanu *et al*., 2011; Li *et al*., 2021). Among the most concerning pollutants are heavy metals, substances with high density and molecular mass that can accumulate in the environment and be absorbed by living organisms, promoting phenomena such as bioaccumulation and biomagnification throughout food chains (Tchounwou *et al*., 2012; Kahlon *et al*., 2014; Bonsignore *et al.,* 2018). Among these elements, zinc stands out as the 23rd most abundant in the Earth's crust and is widely distributed across environmental compartments. Its main emission sources are associated with industrial and agricultural practices, such as mining, smelting, waste incineration, fertilizer use, and pesticide application (Broadley *et al*., 2007; Cloquet *et al*., 2008; Li *et al*., 2011; Tsonev; Cebola Lidon, 2012).

Conventional methods used in water and wastewater treatment, such as

coagulation, flocculation, biological stages, rapid filtration, and disinfection, are insufficient for the selective removal of heavy metals (Pai *et al*., 2020; Saleh *et al*., 2022). Due to this limitation, advanced technologies are gaining ground in the tertiary treatment of heavy metals, including processes such as adsorption (Fagundes-Klen *et al*., 2010), electrocoagulation (Bazrafshan *et al*., 2015), membrane separation (Zeng *et al*., 2016), and photocatalysis (Alshahateet, 2022). Among these alternatives, adsorption stands out for its high efficiency in refining heavy metal concentrations, as well as its ability to operate under various conditions and allow the use of multiple types of adsorbents, both traditional and innovative (Wang *et al*., 2012; Chai *et al*., 2021). In this context, low-cost adsorbent materials, especially those derived from agro-industrial waste, have been explored for the treatment of zinc-containing effluents and can be applied with little or no prior processing (Kurniawan *et al*., 2006). Examples include biomass derived from various agricultural byproducts, such as sawdust, bark, and leaves, due to their carbon-rich lignocellulosic composition (Karim *et al*., 2023).

Rice (*Oryza sativa* L.), a member of the Poaceae family and classified as a monocot, is one of the world's most agriculturally important cereals, alongside maize and wheat (Syuhadah *et al*., 2012; Landi *et al*., 2017). During harvest, rice husks account for approximately 20% of the total grain mass, constituting an abundant byproduct with potential for various technological applications (Kumar *et al*., 2013; Arjmandi *et al*., 2015; Chaudhari *et al*., 2018). This biomass possesses physicochemical characteristics that make it a promising material for adsorption, such as its granular structure, insolubility in aqueous media, significant chemical resistance, and high mechanical robustness, which favor its use in water and wastewater treatment (Ahmaruzzaman, Gupta, 2011; Arena *et al*., 2016). In addition, rice husks possess a protective layer containing between 15 and 20% silica, giving them a special affinity for heavy metals, whose removal occurs primarily through surface complexation and ion exchange processes (Park *et al*., 2023). Due to these properties, the adsorption efficiency of raw rice husks can be enhanced through specific pretreatments and chemical functionalizations, involving impregnation with oxidizing agents and dehydrating substances (Chakraborty *et al*., 2011; Zhang *et al*., 2014).

Although materials analogous to rice husks are commonly used in the removal of heavy metals, most studies reported in the literature focus predominantly on quantifying adsorptive capacity in batch systems, with little attention given to a detailed

analysis of behavior in continuous operations. With regard to rice husks, there is a scarcity of research focused on their performance in fixed-bed columns, including aspects of mass transfer, breakthrough, and kinetic modeling of the process (Agbozu, Emoruwa, 2014; Das, 2024; Yogeshwaran, Priya, 2021). This gap compromises the robustness of the available technical and scientific basis, as it disregards the particularities inherent to the continuous operating regime involving a byproduct with high reuse potential. Consequently, the understanding of the system's behavior remains incomplete under conditions representative of full-scale application, particularly regarding process dynamics along the bed. Given this scenario, the present study aimed to investigate the performance of rice husks functionalized as an adsorbent in the removal of Zn^{2+} in a fixed-bed column, with a focus on design parameters applicable at the full-scale level. To this end, the material was physically and chemically characterized and implemented in a continuous system, based on which the column was sized and kinetically modeled under various operating conditions.

2. MATERIALS AND METHODS

2.1. Preparation and processing of the biomass

Raw rice husks were commercially purchased and subjected to a pretreatment (Scheufele *et al.,* 2016), which consisted of washing the husks with running water and reverse osmosis water, drying them in an oven with convective air circulation at 35 ± 1°C, grinding, and sieving (0.30 and 1.40 mm). The material thus obtained was designated RRH.

2.2. Preparation of zinc solution

To conduct the experiments, synthetic Zn^{2+} solutions were prepared from analytical-grade $ZnCl_2$ salt at concentrations of 3, 4, and 5 meq L^{-1}, via dissolution in reverse osmosis water. Concentrations of NaOH (0.1 mol L^{-1}) and HCl (0.1 mol L^{-1}) were used to adjust the pH of the zinc solutions to a value determined according to the metal speciation diagram. The distribution of Zn^{2+} chemical species as a function of

pH (speciation diagram) was investigated using the Medusa software (Make Equilibrium Diagrams Using Sophisticated Algorithms), via the Hydra interface (Hydrochemical Equilibrium Constant Database). For the simulation, a pH range between 2 and 12 was defined, adopting equilibrium concentrations corresponding to 3, 4, and 5 meq L^{-1}.

2.3. Production of the rice husk adsorbent

The material obtained from the pretreatment (RRH) underwent chemical functionalization via sequential acid and base treatment (Figure 1), following a methodology adapted from Módenes *et al*. (2017) and Schneider *et al.* (2024).

The acid treatment consisted of immersing 10 g of RRH in 1 L of phosphoric acid (H_3PO_4) solution at 1 mol L^{-1} for 30 min at 80 ± 1°C under constant stirring at 100 rpm. After this period, the solid material was separated from the residual liquid using a 45 µm mesh sieve and dried in a forced-convection oven at 105 ± 1°C for 24 h. The dried material was washed with running water and reverse osmosis water, and subjected to alkaline treatment. In this step, the same treatment procedure was followed, but now using 1 L of sodium hydroxide (NaOH) solution at 1.0 mol L^{-1} and at room temperature (approximately 30°C).

After further separation and drying for 24 h, the material was washed again with running water and reverse osmosis water to remove any remaining base residues, and then kept for another 24 h in an oven at 105 ± 1°C to ensure complete removal of residual moisture. The adsorbent resulting from the functionalization of rice husks with acid and base treatment was named FRH.

Figure 1. Production of FRH adsorbent

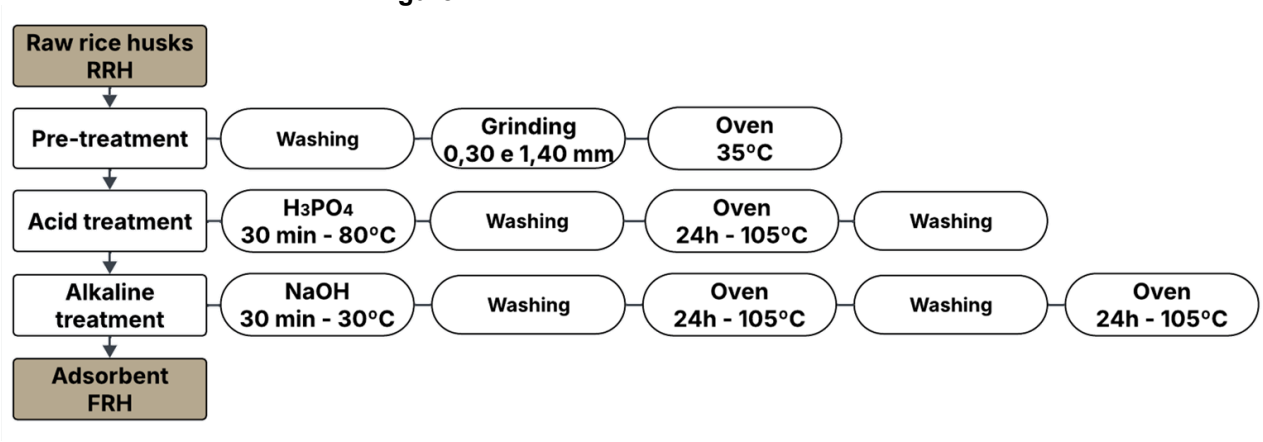

Source: Authors (2026)

2.4. Characterization of the materials

The pretreated raw biomass (RRH) and the chemically functionalized adsorbent (FRH) were characterized using point of zero charge (pH_{PZC}) and Fourier Transform Infrared Spectroscopy (FTIR) techniques to evaluate the structural differences between the original and modified materials.

2.4.1. Point of zero charge

The evaluation of the electrical charge profile present on the surface of RRH and the FRH adsorbent was performed based on the determination of point of zero charge (pH_{PZC}), according to the acid-base titration procedure described by Davranche *et al.* (2003) and based on the surface complexation model developed by Stumm (1992), with methodological adaptations. To this end, 5.0 g of each material were added to Erlenmeyer flasks containing 125 mL of sodium nitrate ($NaNO_3$) solution at 0.1 mol L^{-1}, with an initial pH close to neutrality (7.0). In one sample, titration was performed with nitric acid (HNO_3) at 0.1 mol L^{-1}, while in the other, titration was performed with sodium hydroxide (NaOH) at 0.1 mol L^{-1}. The volume added and the corresponding pH were continuously monitored throughout the entire process. The analyses were conducted over a pH range of 2 to 12, starting from an initial condition close to neutrality. From this point, the system was subjected to two variation trajectories: acidification, achieved by the controlled addition of acidic solution up to

pH 2, and alkalization, performed by the addition of alkaline solution until pH 12. Based on the difference in added volumes and the corresponding pH values, it was possible to estimate the surface charge (Q), expressed in mol g^{-1}, using Eq. (1).

$$Q = \frac{(C_a - C_b) + [OH^-] - [H^+]}{C_s} \quad (1)$$

Where C_a and C_b are the concentrations of HNO_3 and NaOH (mol L^{-1}), respectively, C_s is the concentration of adsorbent (g L^{-1}), and $[OH^-]$ and $[H^+]$ are the concentrations of hydroxide and hydrogen ions in solution (mol L^{-1}), in that order. In the acid titration, C_b was set to zero, whereas in the base titration, C_a was zero.

2.4.2. Surface groups

The characterization of the functional groups present on the surface of RRH and the FRH adsorbent was performed using Fourier Transform Infrared Spectroscopy (FTIR), employing the PerkinElmer FTIR/NIR Spectrometer. The analysis followed the diffuse reflectance method in a potassium bromide (KBr) matrix, as described by Madejová (2003). Each material (RRH, FRH, and KBr) was first dried in an oven at 105 ± 1°C for 24 h and ground to a particle size of less than 50 μm; the pellets were prepared with 0.005 g of adsorbent and 0.1 g of KBr. To acquire the spectra, 32 scans were performed with a spectral resolution of 4.0 cm^{-1}, covering the spectral range between 4000 and 450 cm^{-1}.

2.5. Fixed-bed column adsorption study

Based on the experimental conditions adopted by Do Nascimento *et al.* (2022) and Gupta and Garg (2019), fixed-bed column tests were conducted to study zinc removal. For this purpose, a glass column 30 cm tall, with an internal diameter of 1 cm and an external diameter of 3 cm, was used, resulting in a cross-sectional area of 0.7854 cm^2. The experimental setup (Figure 2) consisted of inserting the FRH adsorbent packed inside the column, forming the fixed-bed. The adsorbent material was manually packed into the column in successive fractions, ensuring homogeneous distribution along the bed height. After addition, the bed was lightly compacted by gently

tapping the column to promote settling of the material and minimize the formation of preferential channels. The same packing procedure was adopted for all bed heights evaluated, ensuring experimental reproducibility. The mass of adsorbent used was adjusted proportionally to the bed height (5, 10, and 15 cm), maintaining the same particle size fraction in all tests.

The system was fed with a zinc solution in a continuous upward flow, with a flow rate of 5 mL min^{-1}, controlled by a peristaltic pump and selected based on preliminary tests to balance an adequate hydraulic residence time with an acceptable pressure drop in the packed bed. To ensure uniform fluid distribution and minimize preferential channels, 0.25 cm diameter glass beads were placed at the top and bottom ends of the column. A thin layer of cotton was added between these beads and the packed bed to retain any fine particles of the adsorbent, preventing their discharge with the effluent. The feed solution was maintained at 30 ± 1°C in an ultrasonic bath to ensure thermal stabilization and adequate dispersion of the metal.

In these experiments, the effect of the initial zinc concentration and bed height on zinc removal efficiency was evaluated by varying the initial concentration of the metal solution (3, 4, and 5 meq L^{-1}) for a 15 cm bed height, and the adsorbent bed height (5, 10, and 15 cm) for 5 meq L^{-1} of zinc. This approach allowed for the independent analysis of each factor on the sizing parameters and the modeling of the adsorption process. Samples were collected at regular intervals throughout the column's operating time, which ranged from 1 minute until saturation, for subsequent determination of the residual zinc concentration in the liquid phase.

Figure 2. Fixed-bed adsorption system

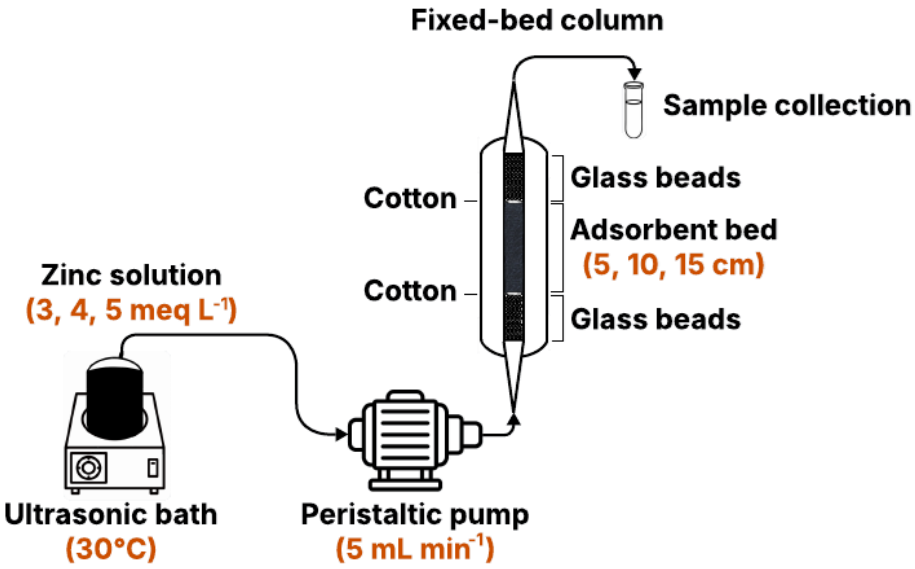

Source: Authors (2026)

2.5.1. Quantification of zinc

The concentration of zinc present in the column effluent was determined using Energy-Dispersive X-ray Fluorescence Spectrometry (EDX). The collected solutions were stored in polypropylene sample bottles and analyzed in analytical duplicate on a Shimadzu EDX-7200 benchtop spectrometer, equipped with a 10 mm collimator and operating in an air atmosphere. Instrumental parameters included an acceleration voltage of 50 kV and automatically adjusted current. The effective acquisition time was 100 seconds, with a dead time of 30% established, considered ideal for ensuring good spectral counting without overloading the detection system. Zinc quantification was performed specifically in the energy range of 8.44 to 8.84 keV, corresponding to the element's Kα line emission. Readings were taken on the channel dedicated to Zn, with accumulated pulses recorded over intervals of up to 40 seconds.

2.6. Column sizing

After determining the zinc concentrations, breakthrough curves were plotted by correlating C/C_0 and t (min), based on which the columns were sized and their kinetics modeled using OriginPro v.10.3 software. The working capacities of the adsorbent

bed, both at the saturation point (q_s) and at breakthrough (q_b), expressed in meq g^{-1}, were obtained based on a mass balance applied to the fixed-bed system. These parameters were calculated using Eq. (2) and Eq. (3), as described by Borba *et al.* (2008), Cren *et al.* (2009), and Do Nascimento *et al.* (2022). The integrals in the expressions can be solved analytically using a polynomial approximation of the concentration-time function, or by numerical integration via the trapezoidal rule, allowing for the accurate estimation of the areas under the experimental curves (Da Silva *et al*., 2002).

$$q_s = \frac{C_0 F}{m} \int_0^{t_{s,u}} \left(1 - \frac{C}{C_0}\right) d_t - \frac{V_t \varepsilon_L C_0}{m} \quad (2)$$

$$q_b = \frac{C_0 F}{m} \int_0^{t_{b,u}} \left(1 - \frac{C}{C_0}\right) d_t - \frac{V_t \varepsilon_L C_0}{m} \quad (3)$$

Where C_0 and C correspond, respectively, to the solute concentrations in the feed and in the column effluent (meq L^{-1}), m represents the mass of adsorbent used (g), F is the volumetric effluent flow rate (L min^{-1}), V_t refers to the total volume occupied by the bed (L), and ε_B indicates the porosity of the bed. The instantaneous saturation time of the column, t_s (min), corresponds to the moment when the ratio C/C_0 reaches a value of 1, while the breakthrough time, t_b (min), was defined as the time when C/C_0 equals 0.01. This criterion was based on a conservative and regulatory approach. The choice is justified by the fact that zinc levels above 3 mg L^{-1} (0.09 meq L^{-1}) can compromise the organoleptic quality of water, giving it turbidity and a metallic taste, according to guidelines from the World Health Organization (WHO, 2011). At the same time, the value complies with the discharge limit of 5 mg L^{-1} (0.15 meq L^{-1}) established by CONAMA Resolution No. 430 (BRAZIL, 2011). Thus, as can be seen in Table 1, the column outlet concentrations remained within both criteria for all experimental conditions.

Table 1. Zinc concentration at the beginning and at column rupture (C/C_0 = 0.01), in meq L^{-1} and mg L^{-1}

Initial zinc concentration (C_0)		Final zinc concentration (C)	
meq L^{-1}	Corresponding value in mg L^{-1}	meq L^{-1}	Corresponding value in mg L^{-1}
3	98.07	0.03	0.9807
4	130.76	0.04	1.3076
5	163.45	0.05	1.6345

Source: Authors (2026)

The efficiency of the adsorption column (η) (%), based on the process's useful saturation and breakthrough capacities, was predicted using Eq. (4) (Yagub *et al.*, 2015).

$$\eta = \frac{q_b}{q_t} 100 \tag{4}$$

The useful bed saturation time ($t_{s,u}$) and the useful breakthrough time ($t_{b,u}$), both expressed in minutes, were determined based on Eq. (5) and Eq. (6), according to the procedures described by Kapur and Mondal (2016) and Juchen *et al.* (2021). The parameter $t_{s,u}$ is related to the area located above the breakthrough curve up to time t_s, while $t_{b,u}$ corresponds to the area bounded up to time t_b, these integrals representing the temporal efficiency of the bed before saturation and breakthrough, respectively.

$$t_{s,u} = \int_0^{t_s} \left(1 - \frac{C}{C_0}\right) d_t \tag{5}$$

$$t_{b,u} = \int_0^{t_b} \left(1 - \frac{C}{C_0}\right) d_t \tag{6}$$

The effective height (H_u) (cm) and the unused height (H_{UNB}) (cm) of the bed were calculated using Eq. (7) and Eq. (8), considering H_t (cm) as the total height. Although H_{UNB} and the mass transfer zone (MTZ) are numerically equivalent, the MTZ corresponds to the region where the main adsorption processes occur, characterized by the concentration gradient between the saturated and unsaturated zones of the bed

(Pereira *et al*., 2006; Kumari *et al*., 2021).

$$H_u = \frac{t_{b,u}}{t_{s,u}} H_t \quad (7)$$

$$H_{UNB} = \mathrm{ZTM} = H_t - H_u \quad (8)$$

The bed porosity (ε_B) was determined using the ratio of the void volume (V_z) (L) to the total column volume (V_t) (L), as expressed in Eq. (9), where V_a is the volume effectively occupied by the adsorbent material (L) (Veit *et al*., 2009; Barquilha *et al*., 2017). The apparent bed density (ρ_B) (g L^{-1}) and the interstitial flow velocity (u_i) (cm min^{-1}) were calculated using Eq. (10) and Eq. (11), respectively. In this case, A_{ST} represents the cross-sectional area of the solution flow within the column (cm^2) (Sulaymon; Ahmed, 2008). Furthermore, the ratio between the mass of adsorbent and the total height of the bed (m_H) (g cm^{-1}) was calculated using Eq. (12).

$$\varepsilon_L = \frac{V_z}{V_t} = \frac{V_t - V_a}{V_t} \quad (9)$$

$$\rho_L = \frac{m}{V_t} \quad (10)$$

$$u_i = \frac{F}{\varepsilon_L A_{ST}} \quad (11)$$

$$m_H = \frac{m}{H_t} \quad (12)$$

2.7. Kinetic modeling of the column

2.7.1. Thomas model

The model proposed by Thomas in 1944 (Thomas, 1944), formalized in Eq. (13), is widely used to describe adsorption dynamics in fixed-bed columns. Its theoretical approach assumes that the system reaches equilibrium according to the Langmuir isotherm and that the kinetics of the process are governed by a second-

order reversible reaction. The application of this model allows for the estimation of the maximum retention capacity of the adsorbate in the solid matrix. However, it disregards any diffusive resistances, both external and intraparticle, which can significantly influence the process performance under real-world conditions (Hu *et al.*, 2019; Patel, 2019).

$$\frac{C}{C_0} = \frac{1}{1+exp\left(k_t\left(\frac{q_T m}{F} - C_0 t\right)\right)} \quad (13)$$

Where k_t is the Thomas kinetic coefficient (L meq^{-1} min^{-1}), q_s is the maximum adsorption capacity predicted by the model (meq g^{-1}), and t is the process time (min) (Ahmed, Hameed, 2018).

2.7.2. Yoon-Nelson model

The model proposed by Yoon and Nelson (Yoon, Nelson, 1984), originally designed to describe the adsorption of gases on activated carbon, is based on the assumption that the solute removal rate depends on both the remaining concentration and the proportion of the bed capacity already utilized. Although its application is limited to systems containing a single component, the mathematical expression associated with the model, presented in Eq. (14), is simplified and does not require detailed data on the specific characteristics of the adsorbate and the adsorbent material (Hamdaoui, 2006; Baral *et al.*, 2009; Jang and Lee, 2016).

$$\frac{C}{C_0} = \frac{exp(k_{YN}t - k_{YN}\tau)}{1+exp(k_{YN}t - k_{YN}\tau)} \quad (14)$$

Where k_{YN} is the Yoon-Nelson kinetic coefficient (min^{-1}) and τ is the adsorption time required for 50% column breakthrough (min) (Hanen, Abdelmottaleb, 2013).

2.7.3. Modified dose-response model

The modified dose-response (MDR) model, proposed by Yan *et al*. (2001), was based on experimental results and statistical analyses related to the biosorption of

heavy metals in continuous systems. As discussed by Song *et al.* (2011), and Xu *et al*. (2013), this approach aims to improve data calibration by correcting distortions observed at extreme time intervals during operation, a common limitation of the Thomas model. Thus, the MDR constitutes a more effective tool for describing adsorption behavior in fixed-beds, ensuring greater accuracy in predicting the saturation of the adsorbent material. The model formulation is presented in Eq. (15).

$$\frac{C}{C_0} = 1 - \frac{1}{1+\left(\frac{C_0 F t}{q_{MDR} m}\right)^{\alpha_{MDR}}} \quad (15)$$

Where α_{MDR} is the MDR exponential rate constant and q_{MDR} represents the maximum adsorption capacity predicted by the model (meq g^{-1}) (Zhao *et al*., 2014).

2.7.4. Adams-Bohart model

The model developed by Adams and Bohart (1920) (Bohart, Adams, 1920) is based on adsorption kinetics governed by a reaction of approximately first order, as can be seen in Eq. (16). This method assumes that the capture rate of the adsorbate is linked both to the concentration of the solute in the liquid phase and to the availability of active sites on the adsorbent material within the column (Malik *et al*., 2018; Zeng *et al*., 2023). Where K_{AB} is the Adams-Bohart kinetic constant (L meq^{-1} min^{-1}) and q_e is equivalent to q_s (meq g^{-1}) (Wang *et al*., 2024).

$$\frac{\partial q\,(t,H_t)}{\partial t} = K_{AB}(q_e - q_{t\,(t,H_t)})C \quad (16)$$

The analytical solution for Eq. (16), developed by Amundson (1948) (Amundson, 1948), is based on the initial conditions and the boundary condition represented by Eqs. (17), (18), and (19), respectively, and is given in Eq. (20).

$$\mathrm{C}\,(0,H_t) = 0 \quad (17)$$

$$\mathrm{q}\,(0,H_t) = 0 \quad (18)$$

$$\mathrm{C}(\mathrm{t},0)=\begin{cases}0, & t=0\\ C_0, & t>0\end{cases} \tag{19}$$

$$\frac{C}{C_0}=\begin{cases}0, & t\ \leq\ \mathrm{t_{res}}\\ \frac{1}{(e^{A_{AB}}+e^{-B_{AB}}-1)e^{B_{AB}}}, & t>t_{res}\end{cases} \tag{20}$$

Where t_{res} denotes the residence time of the adsorbate in the column (min), given by Eq. (21), and A_{AB} and B_{AB} are dimensionless parameters of the Adams-Bohart model, given by Eq. (22) and Eq. (23), respectively. The variables α_{AB} and β_{AB} (min^{-1}) are predicted by Eq. (24) and Eq. (25), in that order (Borba *et al*., 2008).

$$t_{res}=\frac{H_t}{u_i} \tag{21}$$

$$A_{AB}=\frac{H_t\beta_{AB}}{u_i} \tag{22}$$

$$B_{AB}=\frac{(-tu_i+H_t)\beta_{AB}}{\alpha_{AB}u_i} \tag{23}$$

$$\alpha_{AB}=\frac{\rho_L q_e}{C_0\varepsilon_L} \tag{24}$$

$$\beta_{AB}=K_{AB}C_0\alpha_{AB} \tag{25}$$

2.7.5. Bed depth vs. service time model

The bed depth vs. service time (BDST) model, proposed by Hutchins (1973) and based on the Adams-Bohart equation, linearly relates bed height to column operating time, assuming that adsorption is controlled by the reaction at the adsorbent surface. Its mathematical expression, represented by Eq. (26), disregards the effects of external mass transfer resistance and intraparticle diffusion, as is the case for the Thomas model (Taty-Costodes *et al*., 2005; Xu *et al*., 2013; Shanmugam *et al*., 2016; Chu, 2023).

$$\frac{C}{C_0} = \frac{1}{1+exp\left(\frac{K_{BDST}q_e\rho_L H_t}{u_i\varepsilon_L} - K_{BDST}C_0 t\right)} \quad (26)$$

Where K_{BDST} is the BDST kinetic constant (L meq^{-1} min^{-1}) (Dabbagh *et al*., 2016).

2.7.6. Clark model

The model developed by Clark (1987), presented in Eq. (27), describes fixed-bed adsorption using fractional-order kinetics based on the Freundlich isotherm, which is suitable for heterogeneous surfaces and adsorption not limited by a fixed maximum capacity (Hu *et al*., 2024). Furthermore, the model recognizes that mass transfer processes exert a significant influence on the shape of the breakthrough curve. Specifically, diffusion through the fluid film is attributed as the rate-limiting step of the system, indicating that the resistance in transporting the adsorbate to the adsorbent surface is the main factor controlling the adsorption kinetics (Malik *et al*., 2018).

$$\frac{C}{C_0} = \frac{1}{(1+A_C \exp(-r_C t))^{\frac{1}{n_F-1}}} \quad (27)$$

Where A_C is the dimensionless Clark constant, r_C is the kinetic coefficient of the model (min^{-1}), and n_F corresponds to the characteristic exponent of the Freundlich isotherm (Hanbali *et al*., 2014).

2.8. Statistical analysis

The kinetic model that best described the experimental data was evaluated using the coefficient of determination (R^2), the objective function (OF) represented by Eq. (28), and the mean absolute error (MAE) indicated by Eq. (29). Meanwhile, the mean relative deviation (RD_{mean}) (%) between the equilibrium adsorption capacity predicted experimentally ($q_{e,exp}$) and calculated by the model ($q_{e,cal}$) was determined by Eq. (30).

$$OF = \sum_{i=1}^{n}\left(y_i^{exp} - y_i^{mod}\right)^2 \quad (28)$$

$$MAE = \frac{1}{n}\sum_{i=1}^{n}\left|y_i^{exp} - y_i^{mod}\right| \quad (23)$$

$$RD_{mean}\ (\%) = \frac{\left|q_{e,exp} - q_{e,cal}\right|}{q_{e,exp}} 100 \quad (30)$$

Where the terms y^{exp} and y^{mod} correspond, respectively, to the experimentally obtained values of the dependent variable and the values estimated by the model, and n represents the total number of experimental data points

3. RESULTS AND DISCUSSION

3.1. Zinc speciation diagram

The zinc speciation diagram as a function of pH for different initial concentrations of the metal (3, 4, and 5 meq L^{-1}) is shown in Figure 3, from which it can be observed that the metal remains predominantly in the ionic form up to pH 7 for all analyzed concentrations. In more acidic media, especially at pH 5 or lower, the predominant species is the Zn^{2+} cation. As the pH approaches neutrality, between 5 and 8.5, an increasing presence of the $ZnOH^{+}$ ion is observed, whose fraction reaches 0.2 at pH values between 6.9 and 7.1. However, at pH values above 6.9 (3 meq L^{-1}), 7.0 (4 meq L^{-1}), and 6.75 (5 meq L^{-1}), the system begins to favor the formation of zinc oxide (ZnO), which becomes predominant at pH values above 7.5. Therefore, to avoid ranges where metal precipitation could occur, the zinc solutions used for the fixed-bed adsorption experiments were adjusted to pH 5.

Figure 3. Zinc speciation diagram as a function of pH for: (a) 3 meq L^{-1}, (b) 4 meq L^{-1} e (c) 5 meq L^{-1}

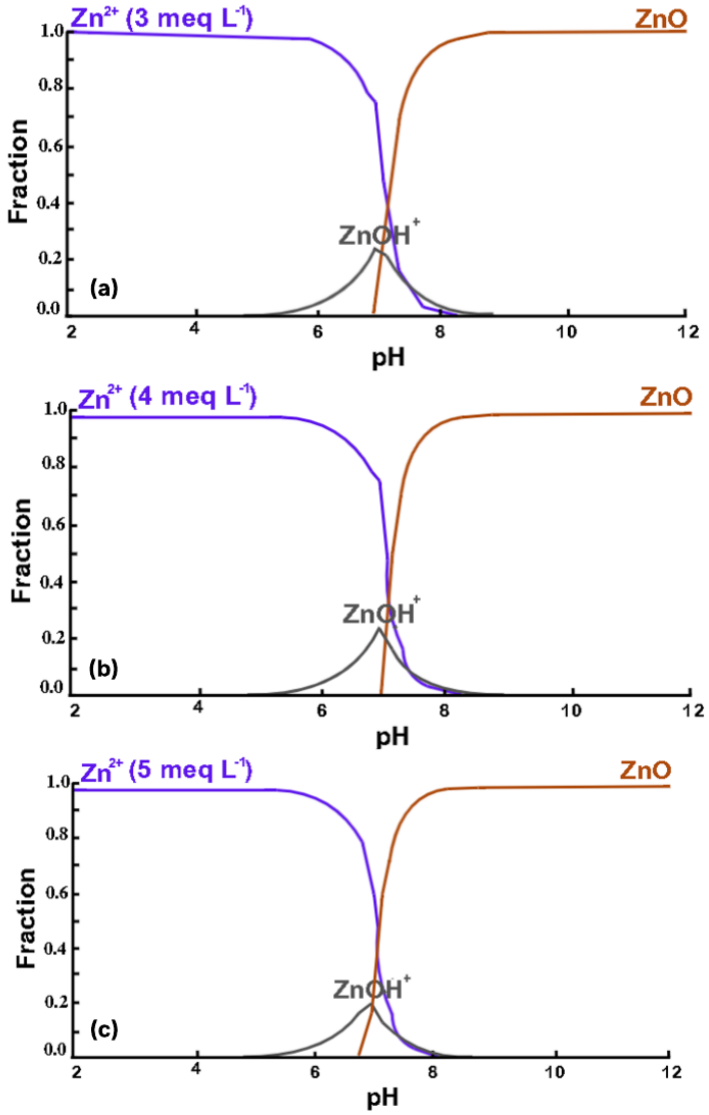

Source: Authors (2026)

3.2. Characterization of the materials

3.2.1. Point of zero charge

Figure 4 shows the distribution of positive and negative charges on RRH and FRH. The analysis of the surface behavior of these materials reveals striking contrasts between the pretreated raw biomass (RRH) and the chemically functionalized adsorbent (FRH). RRH exhibits a broad region near electrochemical neutrality, ranging from pH 3.29 to 10.70, with a point of zero charge (pH_{PZC}) at 6.09. This variation, centered on values close to equilibrium, indicates the prevalence of weak or poorly ionizable functional groups, as commonly observed in non-functionalized

lignocellulosic materials. Consequently, the surface of the natural solid exhibits a low density of charged active sites, which significantly limits interactions with metal species in solution. The pH_{PZC} of RRH was close to those obtained by Banerjee *et al*. (2019) in the analysis of peanut shells (6.21) and almonds (6.10), and by Ouldmoumna *et al*. (2013) in cardoon (*Cynara cardunculus*) (6.25). Regarding raw rice husks, the value reported by El-Shafey *et al.* (2016) was 5.98, while that reported by Lugo-Arias *et al*. (2025) was 6.00, both close to the value recorded in this study.

In contrast, the FRH adsorbent exhibited a charge distribution close to electrochemical neutrality only in the region between pH 8.48 and 10.76, with pHPZC at 9.60 (Figure 4). This difference, when compared to RRH, is associated with the structural modification promoted by the functionalization of FRH with NaOH, which is responsible for the incorporation of alkaline functional groups, such as carboxylates (-COO-) and hydroxyls (OH-), into its cellulose matrix (Beig, Shah, 2023). Although the electrostatic attraction between the surface and zinc cations is theoretically favored at pH values above pH_{PZC} (where the net surface charge of the FHR is negative), metal precipitation becomes predominant in this range (pH > 6.75), as illustrated by the speciation diagram (Figure 3) (Fathy *et al*., 2013; Nizam *et al*., 2022). Therefore, the choice of pH 5 for the fixed-bed tests proved to be strategic: this value ensures the maintenance of zinc in its soluble ionic form, preventing precipitation. It should be noted that the adsorbent's performance is less due to the overall electrostatic attraction, which would be limited by the positive net surface charge of the material at pH 5, and more to specific chemical mechanisms, such as surface complexation and ion exchange. Thus, the direct chemical coordination between the metal and the functional sites of the biomass overcomes the macroscopic electrostatic barrier, maintaining the efficiency of the process (Bhattacharya *et al*., 2006; Pietrobelli *et al*., 2009).

Figure 4. Point of zero charge of RRH and FRH

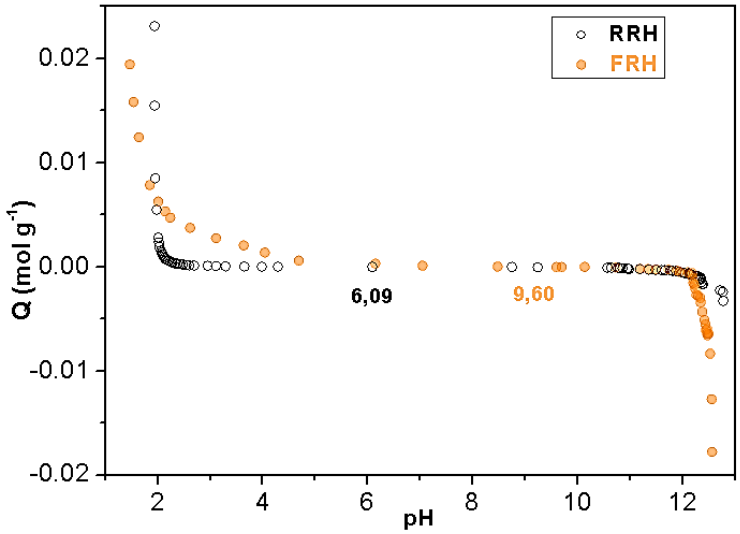

Source: Authors (2026)

3.2.2. Surface groups

Based on the FTIR spectra for RRH and FRH, shown in Figure 5, a broad absorption band is observed at 3438 cm^{-1}, which corresponds to the vibrational stretching of the O–H bond and is characteristic of water molecules, alcohols (cellulose and hemicellulose), and phenols (lignin) (Genieva *et al*., 2008; Armynah *et al*., 2018). Between 1247 and 1126 cm^{-1}, there is stretching of the C–O bond, typical of structural ethers and alcohols in lignin, cellulose, and hemicellulose (Georgakopoulos, 2003; Daffalla *et al*., 2010; Nandiyanto *et al*., 2019). The band at 906 cm^{-1} is associated with the C–O stretching of the β-(1,4) glycosidic bond in cellulose (Yunus, 2019), while the bands at 797, 727, and 656 cm^{-1} result from C–H bending in aromatic structures, such as the guaiacyl (G) and syringyl (S) rings in lignin (Purwaningsih *et al*., 2024).

The peaks at 2938 and 2859 cm^{-1} are associated with the C–H stretching vibrations of alkanes (methyl and methylene) (Abadi *et al*., 2015; Wang *et al*., 2015), while the band at 1750 cm^{-1} is related to the stretching of the C=O bond in carbonyl groups (hemicellulose) and appears exclusively in the RRH sample, evidencing structural modifications resulting from the chemical functionalization process of the FRH adsorbent (Zhang *et al*., 2014). This behavior can be attributed to the formation of the $R–COO^-Na^+$ compound, resulting from the alkaline hydrolysis of esters (R–COO–R) and the ionization of carboxylic acids (R–COOH) in the presence of NaOH. This hypothesis is supported by the bands observed at 1649 and 1438 cm^{-1}, attributed

respectively to the asymmetric and symmetric stretching of the COO^- group, although they may also overlap with vibrations of aromatic compounds and C–H bending of lignin and hemicellulose, such as at 1500 and 1373 cm^{-1} (Oyerinde, Bello, 2016; Hamidu *et al*., 2020; SAITO, Keisuke *et al*., 2022). Consequently, the released Na^+ can act as an exchange cation with Zn^{2+} (Módenes *et al*., 2017).

The spectral regions at 566 and 475 cm^{-1} reflect Si–O bending vibrations of silicate groups present in the cell walls of rice husks (Yu *et al*., 2014; Saudi *et al*., 2015), and the stretching of this bond is observed at 1063 cm^{-1} (Nakbanpote *et al*., 2007; Abadi *et al*., 2015; Mohd Basri *et al*., 2021). Through the functionalization of biomass by combining acid treatment (H_3PO_4) and alkaline (NaOH) treatments, the amorphous silica (SiO_2) released by the acid is depolymerized by the base in the adsorbent's cellulose matrix, generating SiO^- anions on its surface, which can favor the formation of complexes with Zn^{2+} cations (Zn–O–Si) (Anseau *et al*., 2005; Naren *et al*., 2011; CD *et al*., 2013; Shebl *et al*., 2016; Nelson *et al*., 2018). Thus, the characteristic vibrational spectrum of FRH indicates the presence of compounds that favor zinc adsorption, which are not observed in RRH. As a result, there is evidence that ion exchange and surface complexation mechanisms occur in the solid's structure, which may enhance its ability to remove the metal.

Figure 5. FTIR spectra of RRH and FRH

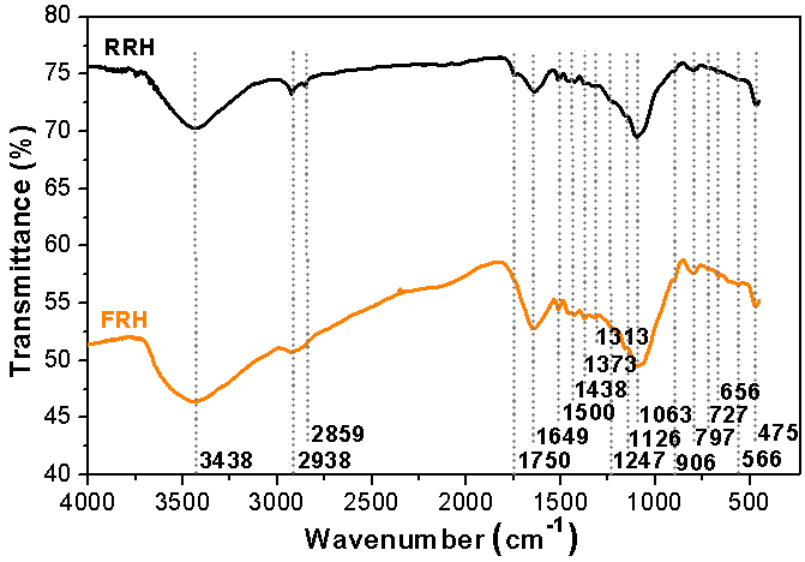

Source: Authors (2026)

3.3. Fixed-bed column

The breakthrough curves resulting from variations in the initial zinc concentration in the column (with a 15 cm bed height) and in the bed height, at a metal concentration of 5 meq L^{-1}, are shown in Figure 6. From these, it can be observed that an increase in the system's initial concentration led to faster column saturation (Figure 6-a), while a decrease in the height of the adsorbent bed, for parameter variations between 5 and 10 cm, accelerated column saturation (Figure 6-b). Both phenomena are corroborated by various authors in the literature (Aichour *et al*., 2019; Renu *et al.*, 2020; Patel, 2020; Khalfa *et al*., 2021).

This behavior is also consistent with the short contact time between the fluid phase and the bed, reflected in the estimated hydraulic residence time, equivalent to 2.36 min, which intensifies the system's sensitivity to the evaluated operating conditions. Furthermore, it is noted that the mass transfer zone in all curves presents an irregular and spread-out shape, a behavior that may be associated with the influence of solute transport resistances, axial dispersion, and possible hydrodynamic non-idealities along the bed. While the theoretical model indicates a well-defined front, real column systems show a gradual change between the start of operation and saturation (Patel, 2019; Taka *et al*., 2021).

Figure 6. Zinc breakthrough curves for (a) H_t of 15 cm and C_0 at 3, 4 and 5 meq L^{-1} and (b) C_0 of 5 meq L^{-1} and H_t at 5, 10 and 15 cm

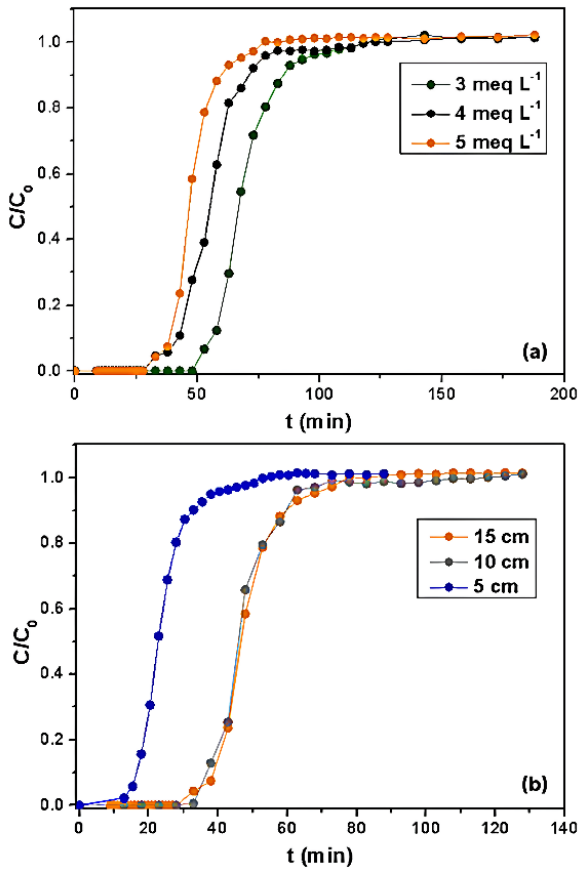

Source: Authors (2026)

3.3.1. Column sizing

The sizing curves for different initial zinc concentrations (Figure 6-a) and bed heights (Figure 6-b) are presented in Table 2 and Table 3, respectively. Although the amount of adsorbent packed in the column was proportional to the established bed height, slight mass adjustments were required to keep the H_t parameter at the desired value. This necessity stems from the heterogeneous nature of the FRH material and its irregular distribution along the column, causing small differences in the measurements of interstitial velocity, porosity, and bed density (Valverde; Griffiths, 2024).

According to Table 2, the increase in the initial zinc concentration resulted in a decrease in the bed's useful saturation time ($t_{s,u}$), a characteristic attributed to the accelerated occupation of the adsorbent's active sites and the earlier exhaustion of the column (Gîlcă *et al.*, 2015). In contrast, the useful breakthrough time ($t_{b,u}$) exhibited distinct behavior at concentrations of 4 and 5 meq L^{-1} , showing a slight increase with

higher metal dosages. This effect may be associated with the mass transfer zone (MTZ) observed at 4 meq L^{-1} (Figure 6-a), which exhibited a slightly narrower profile in the initial stages of the process, leading to an earlier breakthrough. This response underscores the inherent complexity of real adsorption systems, in which mass transfer resistances modulate the shape of the capture front and result in distinct behaviors depending on operating conditions (Patel, 2019).

Table 2. Column sizing for H_t of 15 cm and C_0 at 3, 4 and 5 meq L^{-1}

Parameter	C_0: 3 meq L^{-1}	C_0: 4 meq L^{-1}	C_0: 5 meq L^{-1}
q_s (meq g^{-1})	0,79	0,78	0,83
q_b (meq g^{-1})	0,55	0,40	0,49
$t_{s,u}$ (min)	69,59	55,53	48,11
$t_{b,u}$ (min)	48,60	28,93	29,01
H_u (cm)	10,48	7,81	9,04
H_{UNB}, ZTM (cm)	4,52	7,19	5,96
u_i (cm min^{-1})	16,30	15,31	14,42
ε_B	0,3905	0,4159	0,4414
ρ_B (g L^{-1})	112,90	112,89	113,04
m_H (g cm^{-1})	0,08867	0,08866	0,08878
η (%)	**69,44**	51,24	59,42

Source: Authors (2026)

Table 3. Column sizing for C_0 of 5 meq L^{-1} and H_t at 5, 10 and 15 cm

Parameter	H_t: 5 cm	H_t: 10 cm	H_t: 15 cm
q_s (meq g^{-1})	1,26	1,13	0,83
q_b (meq g^{-1})	0,28	0,76	0,49
$t_{s,u}$ (min)	23,97	47,61	48,11
$t_{b,u}$ (min)	5,63	33,04	29,01
H_u (cm)	1,19	6,94	9,04
H_{UNB}, ZTM (cm)	3,81	3,06	5,96
u_i (cm min^{-1})	13,16	12,50	14,42
ε_B	0,4838	0,5093	0,4414
ρ_B (g L^{-1})	111,28	123,76	113,04
m_H (g cm^{-1})	0,08740	0,0972	0,08878
η (%)	22,24	**68,87**	59,42

Source: Authors (2026)

In contrast, as shown in Table 3, the increase in bed height, accompanied by an increase in adsorbent mass, prolonged the useful saturation time ($t_{s,u}$) of the bed, as corroborated by Kalavathy *et al*. (2010). On the other hand, the useful breakthrough time ($t_{b,u}$) showed a slight reduction between bed heights of 10 and 15 cm, which may be related to limitations in intraparticle transport and the occurrence of hydrodynamic heterogeneities, such as stagnation zones or preferential pathways, in longer columns (Kamolpornwijit *et al*., 2003; Knox *et al.*, 2016; Mestri *et al.*, 2023). Furthermore, in

beds with lower compaction and under higher interstitial velocities, as observed in the 15 cm configuration, axial dispersion tends to occur more irregularly, whereas the absence of a dense structure favors marked variations in the longitudinal concentration profile, which reduces flow uniformity and leads to an earlier breakthrough point (Yun *et al*., 2004; Taheri *et al*., 2012; Igwegbe *et al*., 2021).

The parameter associated with the mass transfer zone (MTZ), corresponding to the unusable fraction of the bed (H_{UNB}), was higher at a concentration of 4 meq L^{-1} (7.19 cm) compared to those obtained for 3 meq L^{-1} (4.52 cm) and 5 meq L^{-1} (5.96 cm), indicating greater dispersion and elongation of the adsorption profile at the intermediate zinc concentration, which resulted in lower utilization of the material along the column (Mesfer *et al*., 2020). Similarly, in the test conducted with a 5 cm bed, the ZTM reached 3.81 cm, a value substantially higher than that observed for 10 cm (3.06 cm) and 15 cm (5.96 cm), revealing a considerably diffuse adsorption front, given the difference in height between each system.

The total and breakthrough capacities of the column (q_s and q_b) varied according to the initial zinc concentration (Table 2). Consequently, efficiencies of 69.44%, 51.24% and 59.42% were obtained for the tests with metal concentrations of 3, 4, and 5 meq L^{-1}, respectively. These performance values, in turn, were higher than those reported by other authors regarding zinc adsorption in a column. This is the case for De Freitas *et al.* (2017), using expanded vermiculite (2.9% at 4 meq L^{-1}, 10.1% at 6 meq L^{-1}, 3.4% at 8 meq L^{-1}), and for Manninen *et al*. (2024), using activated steel mill residues (17.5% at 2.5 meq L^{-1}, 13.1% at 3 meq L^{-1}). Therefore, the efficiency of the FRH bed proved satisfactory, especially for the initial zinc concentration of 3 meq L^{-1}.

Similarly, the parameters q_s and q_b showed considerable differences depending on the bed height (Table 3), with efficiencies of 22.24%, 68.87%, and 59.42% obtained for the 5, 10 and 15 cm columns, respectively. These results were found to be relevant when compared to studies reported in the literature for the same biomass, especially for the 10 cm bed height. This is the case with the research conducted by Alalwan *et al*. (2018) on the adsorption of Ti^{3+} ions by raw rice husks (0.33%, at 5 and 7 cm), and by Vieira *et al.* (2014) on the removal of Pb^{2+} (45.2%, at 14 cm) and Cu^{2+} (39.2%, at 14 cm) using rice husk ash.

Based on these findings, the most favorable column adsorption conditions were

obtained from an initial zinc concentration of 3 meq L^{-1} (15 cm) and a bed height of 10 cm (5 meq L^{-1}), with estimated efficiencies of 69.44% and 68.87%, respectively. These values were higher than those reported in the literature, even under conditions where the breakthrough time was estimated at a higher C/C_0 ratio. Based on this, it is evident that both the concentration of the metal solution and the bed length are determining factors for column performance, directly influencing the total and useful capacity of the system.

3.3.2. Kinetic modeling of the column

The kinetic modeling of the breakthrough curves for different initial zinc concentrations and bed heights is presented in Table 4 and Table 5, respectively. It is observed that all evaluated models were able to satisfactorily describe the experimental profiles of the breakthrough curves under the different conditions studied and that the statistical parameters of Thomas and Yoon-Nelson were similar, whereas both equations are mathematically equivalent for single-component adsorption systems. However, the MDR formulation showed more consistent performance in the 15 cm column at concentrations of 4 and 5 meq L^{-1}, as well as for the initial solution containing 5 meq L^{-1} of zinc in 5 and 10 cm beds. Under these conditions, higher coefficients of determination (R^2), accompanied by lower values of the objective function (OF) and the mean absolute error (MAE), were observed.

In the MDR model, the α_{MDR} parameter is associated with the slope of the breakthrough curve, governing the thickness of the mass transfer zone (MTZ) and reflecting the degree of homogeneity of adsorption across the bed. This becomes evident in the linearized form of the model (Eq. (31)), where αMDRcorresponds to the slope of the line (Ordoñez *et al*., 2022; Viotti *et al*., 2024). Therefore, lower values of αMDR are related to a less abrupt and more diffuse adsorption front, as confirmed by the shape of the MTZ for the 5 cm bed at 5 meq L^{-1} (α_{MDR}: 6.58) (Figure 6-b) and the 15 cm bed at 4 meq L^{-1} (α_{MDR}: 8.57) (Figure 6-a).

$$ln\left(\frac{C}{C_0-C}\right) = \alpha_{MDR}\, ln(C_0 Ft) - \alpha_{MDR} ln\,(mq_{MDR}) \quad (31)$$

Table 4. Column kinetic parameters for H_t of 15 cm and C_0 at 3, 4 and 5 meq L^{-1}

Model	Parameters	C_0: 3 meq L^{-1}	C_0: 4 meq L^{-1}	C_0: 5 meq L^{-1}
Thomas	k_t (L meq^{-1} min^{-1})	0,05 ± 0,00	0,04 ± 0,00	0,05 ± 0,00
	q_s (meq g^{-1})	0,78 ± 0,00	0,78 ± 0,00	0,83 ± 0,00
	R^2	0,9983	0,9990	0,9982
	OF	0,0148	0,0092	0,0121
	MAE	0,0114	0,0109	0,0109
Yoon-Nelson	k_{YN} (min^{-1})	0,16 ± 0,01	0,16 ± 0,00	0,23 ± 0,01
	τ (min)	67,96 ± 0,25	54,88 ± 0,20	47,24 ± 0,23
	R^2	0,9983	0,9990	0,9982
	OF	0,0148	0,0092	0,0121
	MAE	0,0116	0,0108	0,0110
MDR	α_{MDR}	10,85 ± 0,28	**8,57 ± 0,23**	**10,85 ± 0,35**
	q_{MDR} (meq g^{-1})	0,78 ± 0,00	**0,78 ± 0,00**	**0,82 ± 0,00**
	R^2	0,9991	**0,9991**	**0,9992**
	OF	0,0075	**0,0079**	**0,0079**
	MAE	0,0081	**0,0074**	**0,0089**
Adams-Bohart	K_{AB} (L meq^{-1} min^{-1})	0,05 ± 0,00	0,04 ± 0,00	0,05 ± 0,00
	R^2	0,9972	0,9983	0,9981
	OF	0,0248	0,0094	0,0128
	MAE	0,0121	0,0109	0,0107
BDST	K_{BDST} (L meq^{-1} min^{-1})	0,05 ± 0,00	0,04 ± 0,00	0,05 ± 0,00
	R^2	0,9982	0,9990	0,9964
	OF	0,0159	0,0094	0,0165
	MAE	0,0113	0,0108	0,0121
Clark	A_C	**44,13 ± 0,77**	1171,68 ± 68	320 ± 11,02
	r_C (min^{-1})	**0,11 ± 0,01**	0,14 ± 0,01	0,17 ± 0,02
	n_F	**1,03 ± 0,01**	1,66 ± 0,06	1,15 ± 0,07
	R^2	**0,9994**	0,9991	0,9987
	OF	**0,0055**	0,0083	0,0079
	MAE	**0,0066**	0,0090	0,0090

Source: Authors (2026)

The maximum adsorption capacity estimated by the model (q_{MDR}) was found to be considerably close to the experimentally calculated value (q_e). This agreement is attributed to the fact that the MDR equation explicitly accounts for the influence of medium heterogeneity on the process kinetics, allowing the breakthrough curve to be adjusted to adequately represent both the diffusion-governed stages and those associated with the saturation of the adsorbent bed (Song *et al.*, 2011; Xu *et al.*, 2013). The mean relative deviation (RD_{mean}) between the theoretical and experimental parameters, for each evaluated configuration, is shown in Table 6, with the largest deviation observed for the 5 cm column at 5 meq L^{-1} (3.17%). In this arrangement, q_{MDR} presented the best value among the analyzed conditions, equivalent to

1.22 meq g^{-1}, while α_{MDR} reached a magnitude of 6.58. Both constants were higher than those reported by other authors, as shown in Table 7. However, this analysis is qualitative in nature, since factors such as initial concentration, flow rate, bed height, and the nature of the metal directly influence the model parameters.

Table 5. Column kinetic parameters for C_0 of 5 meq L^{-1} and H_t at 5, 10 and 15 cm

Model	Parameters	H_t: 5 cm	H_t: 10 cm	H_t: 15 cm
Thomas	k_t (L meq^{-1} min^{-1})	0,06 ± 0,00	0,05 ± 0,00	0,05 ± 0,00
	q_s (meq g^{-1})	1,24 ± 0,01	1,12 ± 0,01	0,83 ± 0,00
	R^2	0,9934	0,9957	0,9982
	OF	0,0147	0,0171	0,0121
	MAE	0,0207	0,0170	0,0109
Yoon-Nelson	k_{YN} (min^{-1})	0,29 ± 0,02	0,23 ± 0,01	0,23 ± 0,01
	τ (min)	23,08 ± 0,21	46,45 ± 0,31	47,24 ± 0,23
	R^2	0,9934	0,9962	0,9982
	OF	0,0148	0,0171	0,0121
	MAE	0,0209	0,0169	0,0110
MDR	α_{MDR}	**6,58 ± 0,18**	**10,63 ± 0,57**	**10,85 ± 0,35**
	q_{MDR} (meq g^{-1})	**1,22 ± 0,01**	**1,11 ± 0,01**	**0,82 ± 0,00**
	R^2	**0,9984**	**0,9973**	**0,9992**
	OF	**0,0046**	**0,0124**	**0,0079**
	MAE	**0,0123**	**0,0136**	**0,0089**
Adams-Bohart	K_{AB} (L meq^{-1} min^{-1})	0,06 ± 0,00	0,05 ± 0,00	0,05 ± 0,00
	R^2	0,9858	0,9906	0,9981
	OF	0,0423	0,0436	0,0128
	MAE	0,0270	0,0198	0,0107
BDST	K_{BDST} (L meq^{-1} min^{-1})	0,06 ± 0,00	0,05 ± 0,00	0,05 ± 0,00
	R^2	0,9902	0,9943	0,9964
	OF	0,0222	0,0263	0,0165
	MAE	0,0236	0,0170	0,0121
Clark	A_C	0,65 ± 0,02	423,32 ± 18,85	320 ± 11,02
	r_C (min^{-1})	0,20 ± 0,01	0,17 ± 0,02	0,17 ± 0,02
	n_F	1,01 ± 0,00	1,20 ± 0,11	1,15 ± 0,07
	R^2	0,9970	0,9973	0,9987
	OF	0,0058	0,0125	0,0079
	MAE	0,0135	0,0139	0,0090

Source: Authors (2026)

Although the MDR model indicated a high adsorption capacity for the 5 cm column at 5 meq L^{-1}, with good agreement with the experimental value (q_e), this result did not translate into high operational performance of the system. For this condition, the removal efficiency was only 22.24%, showing that the maximum capacity estimated by the model essentially represents the intrinsic potential of the material, while the removal efficiency is directly associated with the utilization of the bed over the

operating time. Thus, it is observed that a high adsorption capacity does not necessarily imply better process performance in continuous regime, since hydrodynamic limitations and the rapid formation of the mass transfer zone can significantly reduce the overall efficiency of the column.

Table 6. Average relative deviation between q_e and q_{MDR}

C_0 (meq L^{-1})	H_t (cm)	q_e (meq g^{-1})	q_{MDR} (meq g^{-1})	RD_{mean} (%)
3	15	0,79	0,78	1,27
4	15	0,78	0,78	0,00
5	15	0,83	0,82	1,20
5	5	1,26	1,22	3,17
5	10	1,13	1,11	1,77

Source: Authors (2026)

On the other hand, Clark's model showed the best fit with the breakthrough curve from 15 cm to 3 meq L^{-1}, achieving a high coefficient of determination (0.9970), low OF error (0.0055), and a reduced MAE parameter value (0.0066). Its formulation adopts the assumptions of the Freundlich batch isotherm (heterogeneous surface, $n_F > 1$) and assumes that mass transfer resistance in the fluid film is the rate-limiting step of the process, allowing the dynamic behavior of the column to be estimated (Vázquez *et al*., 2009). The parameter n_F, related to the intensity of the adsorption process, was incorporated into the model as an adjustable constant, with a value of 1.03, and characterized favorable behavior for zinc removal. This approach helps reduce operational discrepancies, considering that in a batch system the initial solute concentration decreases gradually, while in continuous-flow columns it remains practically stable (Hu *et al*., 2020).

The constant r_C (0.11 min^{-1}), which represents the adsorption rate along the column, also indicates the slope of the MTZ on the breakthrough curve, as corroborated by the linearization of the Clark model (Eq. (32)), in which the parameter corresponds to the slope of the line (Faraj *et al*., 2020; Futalan, Wan, 2022; Din *et al*., 2024; Pan, Zhang, 2025). Its magnitude is supported by the shape of the adsorption front observed in the 15 cm at 3 meq L^{-1} setup (Figure 6-a) and is relatively high when compared to other studies in the literature, as shown in Table 8, whose analysis is qualitative. The coefficient A_C (44.13), present in the independent term of Eq. (32), is related to the initial conditions of the system and the bed capacity prior to the breakthrough point, increasing exponentially with r_C and t_b and decreasing gradually

with the breakthrough concentration (Xu *et al*., 2013; Wang *et al*., 2015).

$$ln\left[\left(\frac{C_0}{C}\right)^{n-1} - 1\right] = r_c t - ln\,(A_c) \quad (32)$$

Table 7. MDR model parameters in different studies in the literature

Metal	Adsorbent	Operating conditions	MDR parameters	Reference
Th^{4+}	Orange peels	F: 6 mL min^{-1} C_0: 0,95 meq L^{-1} H_t: 6 cm	q_{MDR}: 0,544 meq g^{-1} α_{MDR}: 1,58 R^2: 0,98	Khamseh, Ghorbanian, 2018
Pb^{2+}	Date seed biochar	F: 1 mL min^{-1} C_0: 1,0 meq L^{-1} H_t: 5 cm	q_{MDR}: 0,438 meq g^{-1} α_{MDR}: 2,7 R^2: 0,95	Mahdi *et al*., 2018
Cr^{6+}	Spruce sawdust	F: 2 mL min^{-1} C_0: 0,00692 meq L^{-1} H_t: 15 cm	q_{MDR}: 0,256 meq g^{-1} α_{MDR}: 2,48 -	Politi, Sidiras, 2020
Cu^{2+}	Activated charcoal from date seeds	F: 8 mL min^{-1} C_0: 1,888 meq L^{-1} H_t: 15 cm	q_{MDR}: 0,120 meq g^{-1} α_{MDR}: 1,99 R^2: 0,92	Mohsen, Ghanim, 2024
Cu^{2+}	Peanut shells	F: 10 mL min^{-1} C_0: 0,472 meq L^{-1} H_t: 10 cm	q_{MDR}: 0,398 meq g^{-1} α_{MDR}: 4,68 R^2: 0,91	Banerjee *et al*., 2019
Cd^{2+}	Date seed biochar	F: 5 mL min^{-1} C_0: 2,0 meq L^{-1} H_t: 10 cm	q_{MDR}: 0,802 meq g^{-1} α_{MDR}: 6,30 R^2: 0,99	Saravanakumar *et al*., 2022
Zn^{2+}	**FRH**	**F: 5 mL min^{-1}** **C_0: 5,0 meq L^{-1}** **H_t: 5 cm**	**q_{MDR}: 1,22 meq g^{-1}** **α_{MDR}: 6,58** **R^2: 0,99**	**This study**

Source: Authors (2026)

Thus, it is observed that the FRH adsorbent bed showed better agreement with the MDR and Clark kinetic models, exhibiting a maximum adsorption capacity (q_{MDR}: 1.22 meq g^{-1}) (5 cm; 5 meq L^{-1}) (Table 5) significantly higher than that reported in similar studies (Table 7), in addition to a high adsorption rate (r_c: 0.11 min^{-1}) (15 cm; 3 meq L^{-1}) (Table 4). The predominance of these adjustments indicates that the column's behavior was influenced by hydrodynamic phenomena and resistance to solute transport, evidenced by irregular mass transfer zones, gradual saturation progression, and more dispersed rupture profiles. Under these conditions, the MDR model showed a greater capacity to describe the non-homogeneous propagation of the adsorption front, a characteristic associated with axial dispersion, channeling, and internal diffusional limitations. In contrast, Clark's formulation proved compatible with the non-uniform energy distribution of the active sites and the predominance of

resistance in the outer film, aspects consistent with the surface heterogeneity of the material and with the experimental behavior observed during continuous operation (Faraj e*t al*., 2020; Viotti *et al*., 2024).

These results demonstrate the material's significant performance in removing Zn^{2+} ions in a continuous system, with kinetic parameters that outperform those described in the literature. Compared with previous studies involving rice husks, this work included a comprehensive analysis of the material's behavior under continuous conditions and provided relevant parameters for future industrial-scale applications in the treatment of effluents containing heavy metals.

Table 8. Clark model parameters in different studies in the literature

Metal	Adsorbent	Operating conditions	Clark parameters	Reference
Zn^{2+}	Mushroom biochar	F: 1,6 mL min^{-1} C_0: 6 meq L^{-1} H_t: 2,5 cm	A_c: 6,38 r_c: 0,028 min^{-1} n_F:1,60 R^2: 0,99	Abdallah *et al*., 2019
Cu^{2+}	Rice husks	F: 15 mL min^{-1} C_0: 0,315 meq L^{-1} H_t: 10 cm	A_c: 571,92 r_c: 2,013 min^{-1} n_F: 2,0 R^2: 0,99	Sarma *et al*., 2015
Ni^{2+}	Pomegranate peels	F: 8 mL min^{-1} C_0: 0,403 meq L^{-1} H_t: 18 cm	A_c: 0,57 r_c: 0,006 min^{-1} n_F: 1,17 R^2: 0,95	Nourmohammadi Dehbalaei *et al*., 2025
Cr^{6+}	Modified peanut shells	F: 7 mL min^{-1} C_0: 5,7 meq L^{-1} H_t: 2,2 cm	A_c: 437,1 r_c: 0,093 min^{-1} n_F: 2,54 R^2: 0,99	Ma *et al*., 2020
Cu^{2+}	Coconut shells	F: 10 mL min^{-1} C_0: 0,315 meq L^{-1} H_t: 15 cm	A_c: 2,32 r_c: 0,003 min^{-1} n_F: 2,22 R^2: 0,99	Acheampong *et al*., 2013
Pb^{2+}	Biomass of *Phanerochaete chrysosporium*	F: 14 mL min^{-1} C_0: 0,315 meq L^{-1} H_t: 27,5 cm	A_c: 128,83 r_c: 0,014 min^{-1} n_F: 0,5 R^2: 0,99	Pakshirajan, Swaminathan, 2006
Zn^{2+}	**FRH**	**F: 5 mL min^{-1} C_0: 3,0 meq L^{-1} H_t: 15 cm**	**A_c: 44,13 r_c: 0,11 min^{-1} n_F: 1,03 0,99**	**This study**

Source: Authors (2026)

3.4. Disposal of saturated adsorbent

Regeneration of the saturated adsorbent represents a relevant step for the viability of the process on a continuous scale, potentially enabling both the partial recovery of adsorbed Zn^{2+} and the reuse of the FRH in successive operating cycles. The desorption of heavy metals in biomaterials and lignocellulosic adsorbents is frequently conducted using dilute acidic eluents, such as HCl, H_2SO_4, or HNO_3 at low concentrations, which promote the protonation of active sites and the consequent release of the metal ion (Mckinley, Ghahreman, 2018; Sithole, 2024). Alternatively, concentrated saline solutions, such as NaCl or $CaCl_2$, can also be used for ion shifting, depending on the predominant adsorption mechanism (Muscarella *et al*., 2021). Although regeneration tests were not performed in this study, such approaches are widely used to assess regeneration efficiency, progressive loss of adsorptive capacity, structural stability of the material, and eventual leaching of lignocellulosic matrix components throughout adsorption-desorption cycles (Lindholm-Lehto, 2019; Charazińska *et al*., 2022).

When chemical regeneration is not technically efficient or when a sharp drop in adsorptive capacity occurs after multiple cycles, the saturated adsorbent should be directed to stabilization strategies and controlled final disposal. In these cases, processes such as encapsulation in a cementitious matrix or inertization can be employed, reducing the mobility of Zn^{2+} and limiting its solubilization under adverse environmental conditions (Chen *et al*., 2009; Liu *et al*., 2023). Alternatively, when technically feasible, zinc recovery can be integrated into hydrometallurgical routes, allowing its reintroduction into production chains (Williamson *et al*., 2020; Ozturk, 2025). In the absence of these alternatives, disposal in licensed industrial landfills remains the final option, provided that current environmental regulations for waste containing potentially toxic metals are met (Krishnan *et al*., 2021).

4. CONCLUSION

This study evaluated the efficiency of functionalized rice husks (FRH) in removing Zn^{2+} ions in a fixed-bed column system, aiming at application in the tertiary treatment of water and wastewater. The results demonstrated the material's high

efficiency in adsorbing the metal under different operating conditions. The FRH adsorbent, enriched with functional groups that enhance affinity for Zn^{2+} ions (SiO^- and $R\text{-}COO^-Na^+$), exhibited high efficiency in metal removal in a fixed-bed column. Tests conducted at pH 5 demonstrated that increasing the initial zinc concentration reduced the bed saturation time, while increasing the column height increased the value of this parameter. Significant efficiencies were observed for beds of 15 cm at 3 meq L^{-1} (69.44%) and 10 cm at 5 meq L^{-1} (68.87%), while a maximum adsorption capacity of 1.22 meq g^{-1} was calculated for the 5 cm bed at 5 meq L^{-1}, as adjusted by the MDR model. These results highlight the potential for using functionalized rice husks (FRH) as an effective and economically viable alternative for the tertiary treatment of water and effluents on a large scale. It is worth noting that, although conducted under controlled conditions, tests with synthetic solutions do not encompass the complexity of real effluents or multicomponent systems. Furthermore, the absence of regeneration, hydraulic, and mechanical stability assessments limits direct application on an industrial scale. Even so, the study provides useful preliminary parameters to guide future pilot-scale tests and technical and economic feasibility analyses.

5. CONSIDERATIONS FOR FUTURE WORK

Future investigations should focus on the transition to continuous operation on a pilot scale, including evaluating the hydraulic behavior of the fixed bed and defining design criteria. Preliminary sizing studies are also recommended, relating adsorptive capacity and adsorbent mass per treated volume, as well as investigating the regeneration and reuse of the adsorbent material. Additionally, the operational stability of the system under dynamic conditions should be evaluated to support the application and feasibility of the process on a larger scale.

ACKNOWLEDGMENTS

The authors thank the Coordination for the Improvement of Higher Education Personnel (CAPES) for financial support and the Multi-User Analysis Center (CAM/NBQ) for the characterization analyses.

LIST OF SYMBOLS

$[OH^-]$, $[H^+]$	Concentration of hydroxyl and hydrogen ions (mol L^{-1})
α_{MDR}	Exponential constant of the MDR model
C	Adsorbate concentration at the column outlet (meq L^{-1})
C_0	Adsorbate concentration at the column inlet (meq L^{-1})
C_A, C_B	Acid and base concentration in the adsorbent titration (mol L^{-1})
C_b	Column breakthrough concentration (meq L^{-1})
C_s	Adsorbent concentration in the titration (mol g^{-1})
RD_{mean}	Mean relative deviation (%)
ε_L	Bed porosity
F	Column feed flow rate (L min^{-1})
H_t	Total bed height (cm)
H_{UNB}	Unused bed height (cm)
H_u	Useful bed height (cm)
K_{AB}	Adams–Bohart kinetic constant (L min^{-1} meq^{-1})
K_{BDST}	BDST kinetic constant (L min^{-1} meq^{-1})
k_t	Thomas kinetic constant (L meq^{-1} min^{-1})
k_{YN}	Yoon-Nelson kinetic constant (min^{-1})
m	Mass of adsorbent in the column (g)
m_H	Ratio between adsorbent mass and total bed height (g cm^{-1})
n	Number of experimental points
η	Column efficiency (%)
n_F	Freundlich adsorption intensity coefficient
Q	Surface charge of the adsorbent (mol g^{-1})
q_s	Useful adsorption capacity at column saturation (meq g^{-1})
q_b	Useful adsorption capacity at column breakthrough (meq g^{-1})
q_e	Equilibrium adsorption capacity (meq g^{-1})
$q_{e,exp}$	Equilibrium adsorption capacity analytically calculated (meq g^{-1})
$q_{e,cal}$	Equilibrium adsorption capacity calculated by the model (meq g^{-1})
q_{MDR}	Maximum MDR adsorption capacity (meq g^{-1})
q_T	Maximum Thomas adsorption capacity (meq g^{-1})
r_C	Clark model parameter (min^{-1})
t	Column adsorption time (s)
t_s	Instantaneous total column time (min)
$t_{s,u}$	Useful total column time (min)
t_b	Instantaneous column breakthrough time (min)
$t_{b,u}$	Useful column breakthrough time (min)
τ	Contact time for 50% column breakthrough (min)
u_i	Interstitial velocity (cm min^{-1})
V_a	Volume of adsorbent in the bed (L)
V_t	Total bed volume (L)
V_z	Void volume in the bed (L)
y_i^{exp}, y_i^{mod}	Parameter experimentally and model calculated
ρ_L	Bed density (g L^{-1})
A_{AB}, B_{AB} α_{AB}, β_{AB}	Adams-Bohart parameters

REFERENCES

ABADI, MH Shahrokh *et al*. Effects of annealing temperature on infrared spectra of SiO_2 extracted from rice husk. **J Ceram Sci Technol**, v. 6, n. 1, p. 41-46, 2015.

ABDALLAH, Maha M. *et al*. Batch and continuous systems for Zn, Cu, and Pb metal ions adsorption on spent mushroom compost biochar. **Industrial & Engineering Chemistry Research**, v. 58, n. 17, p. 7296-7307, 2019.

ACHEAMPONG, Mike A. *et al*. Removal of Cu (II) by biosorption onto coconut shell in fixed-bed column systems. **Journal of Industrial and Engineering Chemistry**, v. 19, n. 3, p. 841-848, 2013.

ADANE, Teshale *et al*. Textile industry effluent treatment techniques. **Journal of Chemistry**, v. 2021, p. 1-14, 2021.

AGBOZU, I. E.; EMORUWA, F. O. Batch adsorption of heavy metals (Cu, Pb, Fe, Cr and Cd) from aqueous solutions using coconut husk. **African Journal of Environmental Science and Technology**, v. 8, n. 4, p. 239-246, 2014.

AHMARUZZAMAN, M.; GUPTA, Vinod K. Rice husk and its ash as low-cost adsorbents in water and wastewater treatment. **Industrial & Engineering Chemistry Research**, v. 50, n. 24, p. 13589-13613, 2011.

AHMED, M. J.; HAMEED, B. H. Removal of emerging pharmaceutical contaminants by adsorption in a fixed-bed column: a review. **Ecotoxicology and Environmental Safety**, v. 149, p. 257-266, 2018.

AICHOUR, Amina *et al*. Low-cost, biodegradable and highly effective adsorbents for batch and column fixed bed adsorption processes of methylene blue. **Journal of Environmental Chemical Engineering**, v. 7, n. 5, p. 103409, 2019.

ALALWAN, Hayder A. *et al.* Adsorption of thallium ion (Ti^{+3}) from aqueous solutions by rice husk in a fixed-bed column: experiment and prediction of breakthrough curves. **Environmental Technology & Innovation**, v. 12, p. 1-13, 2018.

ALSHAHATEET, Solhe. Photocatalytic efficiency of titanium dioxide for dyes and heavy metals removal from wastewater. **Bulletin of Chemical Reaction Engineering & Catalysis**, 2022.

AMUNDSON, Neal R. A note on the mathematics of adsorption in beds. **The Journal of Physical Chemistry**, v. 52, n. 7, p. 1153-1157, 1948.

ANSEAU, Michel R. *et al.* Interactions of silicate ions with zinc (II) and aluminum (III) in alkaline aqueous solution. **Inorganic Chemistry**, v. 44, n. 22, p. 8023-8032, 2005.

ARENA, Noemi *et al*. Life Cycle Assessment of activated carbon production from coconut shells. Journal of Cleaner Production, v. 125, p. 68-77, 2016.

ARJMANDI, Reza *et al*. Rice husk filled polymer composites. **International Journal of Polymer Science**, v. 2015, 2015.

ARMYNAH, Bidayatul *et al*. Analysis of chemical and physical properties of biochar from rice husk biomass. In: **Journal of Physics: Conference Series**. IOP Publishing, 2018. p. 012038.

BANERJEE, Munmun *et al.* Cu (II) removal using green adsorbents: kinetic modeling and plant scale-up design. **Environmental Science and Pollution Research**, v. 26, n. 12, p. 11542-11557, 2019.

BARAL, S. S. *et al.* Removal of Cr (VI) by thermally activated weed Salvinia cucullata in a fixed-bed column. **Journal of Hazardous Materials**, v. 161, n. 2-3, p. 1427-1435, 2009.

BARQUILHA, C. E. R. *et al*. Biosorption of nickel (II) and copper (II) ions in batch and fixed-bed columns by free and immobilized marine algae Sargassum sp. **Journal of Cleaner Production**, v. 150, p. 58-64, 2017.

BAZRAFSHAN, Edris *et al*. Heavy metals removal from aqueous environments by electrocoagulation process–a systematic review. **Journal of Environmental Health Science and Engineering**, v. 13, n. 1, p. 74, 2015.

BEIG, Sajad Ur Rehman; SHAH, Shakeel A. Adsorption of Cr (VI) by NaOH-modified microporous activated carbons derived from the wastes of Amaranthus retroflexus, Magnolia soulangeana, and Tanacetum Vulgar L.: mechanism, isotherms, and kinetic studies. **Environmental Science and Pollution Research**, v. 30, n. 13, p. 35808-35837, 2023.

BHATTACHARYA, A. K. *et al*. Adsorption of Zn (II) from aqueous solution by using

different adsorbents. **Chemical Engineering Journal**, v. 123, n. 1-2, p. 43-51, 2006.

BOHART, G. S.; ADAMS, E. Q. Some aspects of the behavior of charcoal with respect to chlorine. **Journal of the American Chemical Society**, v. 42, n. 3, p. 523-544, 1920.

BONSIGNORE, Maria *et al*. Bioaccumulation of heavy metals in fish, crustaceans, molluscs and echinoderms from the Tuscany coast. **Ecotoxicology and Environmental Safety**, v. 162, p. 554-562, 2018.

BORBA, Carlos Eduardo *et al.* Prediction of the copper (II) ions dynamic removal from a medium by using mathematical models with analytical solution. **Journal of Hazardous Materials**, v. 152, n. 1, p. 366-372, 2008.

BRASIL. Conselho Nacional do Meio Ambiente. **Resolução nº 430, de 13 de maio de 2011**. Dispõe sobre condições e padrões de lançamento de efluentes, complementa e altera a Resolução nº 357, de 17 de março de 2005, do Conselho Nacional do Meio Ambiente (Conama). Brasília, DF: Ministério do Meio Ambiente, 2011.

BROADLEY, Martin R. *et al*. Zinc in plants. **New Phytologist**, v. 173, n. 4, p. 677-702, 2007.

CD, Midhun Dominic *et al*. Synthesis, characterization and application of rice husk nanosilica in natural rubber. **IJST**, v. 2, n. 4, p. 1027-1035, 2013.

CHAI, Wai Siong *et al*. A review on conventional and novel materials towards heavy metal adsorption in wastewater treatment application. **Journal of Cleaner Production**, v. 296, p. 126589, 2021.

CHAKRABORTY, Sagnik *et al*. Adsorption of crystal violet from aqueous solution onto NaOH-modified rice husk. **Carbohydrate Polymers**, v. 86, n. 4, p. 1533-1541, 2011.

CHARAZIŃSKA, Sylwia *et al*. Recent trends in Ni (II) sorption from aqueous solutions using natural materials. **Reviews in Environmental Science and Bio/Technology**, v. 21, n. 1, p. 105-138, 2022.

CHAUDHARI, Prabha R. *et al.* Rice nutritional and medicinal properties: a review article. **Journal of Pharmacognosy and Phytochemistry**, v. 7, n. 2, p. 150-156, 2018.

CHEN, Q. Y. *et al*. Immobilisation of heavy metal in cement-based solidification/stabilisation: A review. **Waste Management**, v. 29, n. 1, p. 390-403, 2009.

CHU, Khim Hoong. Fixed bed adsorption of water contaminants: a cautionary guide to simple analytical models and modeling misconceptions. **Separation & Purification Reviews**, v. 52, n. 2, p. 75-97, 2023.

CLARK, Robert M. Evaluating the cost and performance of field-scale granular activated carbon systems. **Environmental Science & Technology**, v. 21, n. 6, p. 573-580, 1987.

CLOQUET, Christophe *et al*. Variation in the isotopic composition of zinc in the natural environment and the use of zinc isotopes in biogeosciences: a review. **Analytical and Bioanalytical Chemistry**, v. 390, p. 451-463, 2008.

CREN, Érika C. *et al*. Breakthrough curves for oleic acid removal from ethanolic solutions using a strong anion exchange resin. **Separation and Purification Technology**, v. 69, n. 1, p. 1-6, 2009.

DA SILVA, Edson Antonio *et al.* Modeling of copper (II) biosorption by marine alga Sargassum sp. in fixed-bed column. **Process Biochemistry**, v. 38, n. 5, p. 791-799, 2002.

DABBAGH, Reza *et al*. Removal of zinc (II) from synthetic effluent using seaweeds: a review of modeling of fixed-bed columns. **Desalination and Water Treatment**, v. 57, n. 51, p. 24509-24518, 2016.

DAFFALLA, Samah B. *et al.* Characterization of adsorbent developed from rice husk: effect of surface functional group on phenol adsorption. **J. Appl. Sci**, v. 10, n. 12, p. 1060-1067, 2010.

DAS, Shaon Kumar. Agro-waste based biomass residues valorization for effective adsorption of heavy metal. **Environmental Monitoring and Assessment**, v. 196, n. 11, p. 1058, 2024.

DAVRANCHE, Mélanie *et al.* An easy determination of the surface chemical properties of simple and natural solids. **Journal of Chemical Education**, v. 80, n. 1, p. 76, 2003.

DE FREITAS, Emanuelle Dantas *et al*. Binary adsorption of zinc and copper on expanded vermiculite using a fixed bed column. **Applied Clay Science**, v. 146, p. 503-509, 2017.

DIN, Salah Ud *et al*. Enhancing arsenic removal using Cu-infused biochar: Unravelling the influence of pH, temperature and kinetics. **Chemical Engineering Research and Design**, v. 203, p. 368-377, 2024.

DO NASCIMENTO, Cleuciane Tillvitz *et al*. Adsorption of atrazine from aqueous systems on chemically activated biochar produced from corn straw. **Journal of Environmental Chemical Engineering,** v. 10, n. 1, p. 107039, 2022.

EL-SHAFEY O. I. *et al.* Adsorption of Pb ions onto natural and modified egyptian rice husk: kinetic and isotherm equilibrium studies. **Environ. Sci. Ind. J.**, v. 12, n. 9, p.113, 2016.

FAGUNDES-KLEN, Márcia Regina *et al*. Copper biosorption by biomass of marine alga: Study of equilibrium and kinetics in batch system and adsorption/desorption cycles in fixed bed column. **Water, Air, & Soil Pollution**, v. 213, n. 1, p. 15-26, 2010.

FARAJ, Samara Saad *et al.* Simulate permeable reactive barrier by using a COMSOL model and comparison with the Thomas, Yoon–Nelson and Clark models for CR dye remediation by composite adsorbent (sewage and waterworks sludge). **Water Science and Technology**, v. 82, n. 12, p. 2902-2919, 2020.

FATHY, Nady A. *et al.* Effectiveness of Alkali-Acid Treatment in Enhancement the Adsorption Capacity for Rice Straw: The Removal of Methylene Blue Dye. **International Scholarly Research Notices**, v. 2013, n. 1, p. 208087, 2013.

FUTALAN, Cybelle Morales; WAN, Meng-Wei. Fixed-bed adsorption of lead from aqueous solution using chitosan-coated bentonite. **International Journal of Environmental Research and Public Health**, v. 19, n. 5, p. 2597, 2022.

GENIEVA, S. D. *et al*. Characterization of rice husks and the products of its thermal degradation in air or nitrogen atmosphere. **Journal of Thermal Analysis and Calorimetry**, v. 93, p. 387-396, 2008.

GEORGAKOPOULOS, Andreas. Study of low rank Greek coals using FTIR spectroscopy. **Energy Sources**, v. 25, n. 10, p. 995-1005, 2003.

GÎLCĂ, Emilia *et al*. Kinetics analysis of zinc sorption in fixed bed column using a strongly basic anionic exchange resin. **Water Science and Technology**, v. 71, n. 11, p. 1646-1653, 2015.

GUPTA, Anirudh; GARG, Anurag. Adsorption and oxidation of ciprofloxacin in a fixed bed column using activated sludge derived activated carbon. **Journal of Environmental Management**, v. 250, p. 109474, 2019.

HAMDAOUI, Oualid. Dynamic sorption of methylene blue by cedar sawdust and crushed brick in fixed bed columns. **Journal of Hazardous Materials**, v. 138, n. 2, p. 293-303, 2006.

HAMIDU, L. A. J. *et al*. Fourier transform infrared analysis of sawdust and rice husks waste: a raw material for eco-friendly composite production. **Saudi J. Eng. Technol**, v. 5, p. 343-350, 2020.

HANBALI, Mohammad *et al*. Remediation of lead by pretreated red algae: adsorption isotherm, kinetic, column modeling and simulation studies. **Green Chemistry Letters and Reviews**, v. 7, n. 4, p. 342-358, 2014.

HANEN, Nouri; ABDELMOTTALEB, Ouederni. Modeling of the dynamics adsorption of phenol from an aqueous solution on activated carbon produced from olive stones. **Journal of Chemical Engineering & Process** Technology, v. 4, n. 3, 2013.

HU, Qili *et al.* A critical review of breakthrough models with analytical solutions in a fixed-bed column. **Journal of Water Process Engineering**, v. 59, p. 105065, 2024.

HU, Qili *et al*. Development of fractal-like Clark model in a fixed-bed column. **Separation and Purification Technology**, v. 251, p. 117396, 2020.

HU, Qili *et al*. Fractal-like kinetics of adsorption on heterogeneous surfaces in the fixed-bed column. **Chemical Engineering Journal**, v. 358, p. 1471-1478, 2019.

HUTCHINS, Roy A. New method simplifies design of activated carbon systems. **Chem. Eng**., v. 80, p. 133-138, 1973.

IGWEGBE, Chinenye Adaobi *et al.* Environmental protection by the adsorptive elimination of acetaminophen from water: a comprehensive review. **Journal of Industrial and Engineering Chemistry**, v. 104, p. 117-135, 2021.

JANG, Jiseon; LEE, Dae Sung. Enhanced adsorption of cesium on PVA-alginate encapsulated Prussian blue-graphene oxide hydrogel beads in a fixed-bed column system. **Bioresource Technology**, v. 218, p. 294-300, 2016.

JUCHEN, Patricia Trevisani *et al*. Biosorption of dye by malt bagasse in a fixed-bed column: Experimental and theoretical breakthrough curves. **Water, Air, & Soil Pollution,** v. 232, n. 4, p. 128, 2021.

KAHLON, Sharanjeet Kaur *et al*. Impact of heavy metals and nanoparticles on aquatic biota. **Environmental Chemistry Letters**, v. 16, p. 919-946, 2018.

KALAVATHY, Helen *et al*. Removal and recovery of Ni and Zn from aqueous solution using activated carbon from *Hevea brasiliensis*: batch and column studies. **Colloids and surfaces B: Biointerfaces**, v. 78, n. 2, p. 291-302, 2010.

KAMOLPORNWIJIT, W. *et al.* Preferential flow path development and its influence on long-term PRB performance: column study. **Journal of Contaminant Hydrology**, v. 66, n. 3-4, p. 161-178, 2003.

KANU, Ijeoma *et al*. Industrial effluents and their impact on water quality of receiving rivers in Nigeria. **Journal of Applied Technology in Environmental Sanitation**, v. 1, n. 1, p. 75-86, 2011.

KAPUR, Meghna; MONDAL, Monoj Kumar. Design and model parameters estimation for fixed–bed column adsorption of Cu (II) and Ni (II) ions using magnetized saw dust. **Desalination and Water Treatment**, v. 57, n. 26, p. 12192-

12203, 2016.

KARIM, Ahasanul *et al.* Valorization of fibrous plant-based food waste as biosorbents for remediation of heavy metals from wastewater - A review. **Molecules**, v. 28, n. 10, p. 4205, 2023.

KHALFA, Leila *et al*. A calcined clay fixed bed adsorption studies for the removal of heavy metals from aqueous solutions. **Journal of Cleaner Production**, v. 278, p. 123935, 2021.

KHAMSEH, Ali Gh; GHORBANIAN, Sohrab Ali. Experimental and modeling investigation of thorium biosorption by orange peel in a continuous fixed-bed column. **Journal of Radioanalytical and Nuclear Chemistry**, v. 317, n. 2, p. 871-879, 2018.

KNOX, James C. *et al*. Limitations of breakthrough curve analysis in fixed-bed adsorption. **Industrial & Engineering Chemistry Research**, v. 55, n. 16, p. 4734-4748, 2016.

KRISHNAN, Santhana *et al.* Current technologies for recovery of metals from industrial wastes: An overview. **Environmental Technology & Innovation**, v. 22, p. 101525, 2021.

KUMAR, S. *et al*. Utilization of rice husk and their ash: a review. **Res. J. Chem. Env. Sci.**, v. 1, n. 5, p. 126-129, 2013.

KUMARI, Usha *et al*. Effective defluoridation of industrial wastewater by using acid modified alumina in fixed-bed adsorption column: experimental and breakthrough curves analysis. **Journal of Cleaner Production**, v. 279, p. 123645, 2021.

KURNIAWAN, Tonni Agustiono *et al*. Comparisons of low-cost adsorbents for treating wastewaters laden with heavy metals. **Science of the Total Environment**, v. 366, n. 2-3, p. 409-426, 2006.

LANDI, Simone *et al*. Poaceae vs. abiotic stress: focus on drought and salt stress, recent insights and perspectives. **Frontiers in Plant Science**, v. 8, 261997 p., 2017.

LI, Peiyue *et al*. Sources and consequences of groundwater contamination. **Archives of Environmental Contamination and Toxicology**, v. 80, p. 1-10, 2021.

LI, Tingqiang *et al*. Rhizosphere characteristics of zinc hyperaccumulator Sedum alfredii involved in zinc accumulation. Journal of Hazardous Materials, v. 185, n. 2-3, p. 818-823, 2011.

LINDHOLM-LEHTO, Petra C. Biosorption of Heavy Metals by Lignocellulosic Biomass and Chemical Analysis. **BioResources**, v. 14, n. 2, 2019.

LIU, Jingjing *et al*. Review of the interactions between conventional cementitious materials and heavy metal ions in stabilization/solidification processing. **Materials**, v. 16, n. 9, p. 3444, 2023.

LUGO-ARIAS, José *et al*. Removal of nitrate and phosphate from aqueous solutions using bioadsorbents derived from agro-industrial wastes of rice husk and corn stalk. **Biomass Conversion and Biorefinery**, p. 1-23, 2025.

MA, Jie *et al.* Waste peanut shell modified with polyethyleneimine for enhancement of hexavalent chromium removal from solution in batch and column modes. **Bioresource Technology Reports**, v. 12, p. 100576, 2020.

MADEJOVÁ, J. J. V. S. FTIR techniques in clay mineral studies. **Vibrational Spectroscopy**, v. 31, n. 1, p. 1-10, 2003.

MAHDI, Zainab *et al*. Removal of lead (II) from aqueous solution using date seed-derived biochar: batch and column studies. **Applied Water Science**, v. 8, n. 6, p. 181, 2018.

MALIK, Davendra Singh *et al*. Heavy metal removal by fixed-bed column–a review. **ChemBioEng Reviews**, v. 5, n. 3, p. 173-179, 2018.

MANNINEN, Mikael *et al*. Zn (II) removal from wastewater by an alkali-activated material prepared from steel industry slags: optimization and modelling of a fixed-bed process. **Environmental Technology**, v. 45, n. 13, p. 2519-2530, 2024.

MCKINLEY, Caitlyn; GHAHREMAN, Ahmad. Hydrochloric acid regeneration in hydrometallurgical processes: a review. **Mineral Processing and Extractive Metallurgy**, v. 127, n. 3, p. 157-168, 2018.

MESTRI, Safal *et al.* Bromate removal from water using ion exchange resin: batch and fixed bed column performance. **Ozone: Science & Engineering**, v. 45, n. 3, p. 291-304, 2023.

MÓDENES, Aparecido Nivaldo *et al*. Study of the involved sorption mechanisms of Cr (VI) and Cr (III) species onto dried Salvinia auriculata biomass. **Chemosphere**, v. 172, p. 373-383, 2017.

MOHD BASRI, Mohd Salahuddin *et al*. Rice husk ash-based geopolymer binder: Compressive strength, optimize composition, FTIR spectroscopy, microstructural, and potential as fire-retardant material. **Polymers**, v. 13, n. 24, p. 4373, 2021.

MOHSEN, Huda A.; GHANIM, Alaa N. Efficient Removal of Zinc and Copper from Wastewater Using Activated Carbon Derived from Date Pits in a Continuous Fixed-Bed Column. **Journal of Composite & Advanced Materials/Revue des Composites et des Matériaux Avancés**, v. 34, n. 2, 2024.

MUSCARELLA, Sofia Maria et al. Ammonium adsorption, desorption and recovery by acid and alkaline treated zeolite. **Bioresource Technology**, v. 341, p. 125812, 2021.

NAKBANPOTE, Woranan *et al.* Copper adsorption on rice husk derived materials studied by EPR and FTIR. **Colloids and Surfaces A: Physicochemical and Engineering Aspects**, v. 304, n. 1-3, p. 7-13, 2007.

NANDIYANTO, Asep Bayu Dan *et al*. How to read and interpret FTIR spectroscope of organic material. **Indonesian Journal of Science and Technology**, v. 4, n. 1, p. 97-118, 2019.

NAREN, Gaowa *et al.* Formation of a silicato complex of zinc in aqueous solution and its accelerating effect on the formation of silica scales in cooling water systems. **Journal of Colloid and Interface Science**, v. 353, n. 1, p. 331-334, 2011.

NELSON, Joey *et al.* Effects of nano-confinement on Zn (II) adsorption to nanoporous silica. **Geochimica et Cosmochimica Acta**, v. 240, p. 80-97, 2018.

NIZAM, Nurul Umairah M. *et al*. Effective adsorptive removal of dyes and heavy metal using graphene oxide based Pre-treated with $NaOH/H_2SO_4$ rubber seed shells synthetic graphite Precursor: Equilibrium Isotherm, kinetics and thermodynamic studies. **Separation and Purification Technology**, v. 289, p. 120730, 2022.

NOURMOHAMMADI DEHBALAEI, Fereshteh *et al*. Green walnut husk and pomegranate peel for nickel removals from industrial wastewater by absorption process: batch and column experiments. **Applied Water Science**, v. 15, n. 8, p. 1-21, 2025.

ORDONEZ, Diana *et al*. Green sorption media for the removal of perfluorooctanesulfonic acid (PFOS) and perfluorooctanoic acid (PFOA) from water. **Science of the Total Environment**, v. 819, p. 152886, 2022.

OULDMOUMNA, Aoumria *et al.* Characterization and application of three novel biosorbents “Eucalyptus globulus, Cynara cardunculus, and Prunus cerasefera” to dye removal. **Desalination and Water Treatment**, v. 51, n. 16-18, p. 3527-3538, 2013.

OYERINDE, A. Y.; BELLO, E. I. Use of fourier transformation infrared (FTIR) spectroscopy for analysis of functional groups in peanut oil biodiesel and its blends. **British Journal of Applied Science & Technology**, v. 13, n. 3, p. 1-14, 2016.

OZTURK, Yasemin. Selective Recovery of Zinc from Oxide Ores Using Monosodium Glutamate as a Green Lixiviant. **Minerals**, v. 15, n. 8, p. 870, 2025.

PAI, Chih-Wei *et al*. Occurrences of pharmaceuticals and personal care products in the drinking water of Taiwan and their removal in conventional water treatment processes. **Chemosphere**, v. 256, p. 127002, 2020.

PAKSHIRAJAN, K.; SWAMINATHAN, T. Continuous biosorption of Pb, Cu, and Cd by Phanerochaete chrysosporium in a packed column reactor. **Soil and Sediment Contamination: An International Journal**, v. 15, n. 2, p. 187-197, 2006.

PAN, Yanan; ZHANG, Wencai. Enhanced continuous lithium extraction using self-designed porous nanosorbent fibers in a fixed-bed system: Optimization and mechanistic insights. **Desalination**, v. 593, p. 118223, 2025.

PARK, Ji Yeon *et al*. Pilot-scale continuous biogenic silica extraction from rice husk by one-pot alkali hydrothermal treatment and ball milling. **Chemical and Biological Technologies in Agriculture**, v. 10, n. 1, p. 102, 2023.

PATEL, Himanshu. Batch and continuous fixed bed adsorption of heavy metals removal using activated charcoal from neem (Azadirachta indica) leaf powder. **Scientific Reports**, v. 10, n. 1, p. 16895, 2020.

PATEL, Himanshu. Fixed-bed column adsorption study: a comprehensive review. **Applied Water Science**, v. 9, n. 3, p. 45, 2019.

PEREIRA, Milton Rogério *et al*. Chromium adsorption in olive stone activated carbon. **Adsorption**, v. 12, n. 2, p. 155-162, 2006.

PIETROBELLI, Juliana MT de A. *et al.* Cadmium, copper and zinc biosorption study by non-living *Egeria densa* biomass. **Water, Air, and Soil Pollution**, v. 202, n. 1, p. 385-392, 2009.

POLITI, Dororthea; SIDIRAS, Dimitrios. Modified spruce sawdust for sorption of hexavalent chromium in batch systems and fixed-bed columns. **Molecules**, v. 25, n. 21, p. 5156, 2020.

PURWANINGSIH, Sri Yani *et al.* Simultaneous synthesis of silica polymorphs and activated carbon from rice husk. **Silicon**, p. 1-10, 2024.

RENU *et al.* Continuous fixed-bed adsorption of heavy metals using biodegradable adsorbent: modeling and experimental study. **Journal of Environmental Engineering**, v. 146, n. 2, p. 04019110, 2020.

SAITO, Keisuke *et al*. Correlation between C═O Stretching Vibrational Frequency and p Ka Shift of Carboxylic Acids. **The Journal of Physical Chemistry B**, v. 126, n. 27, p. 4999-5006, 2022.

SALEH, Tawfik A. *et al*. Water treatment technologies in removing heavy metal ions from wastewater: A review. **Environmental Nanotechnology, Monitoring & Management**, v. 17, p. 100617, 2022.

SARAVANAKUMAR, Krishnan *et al*. Continuous removal of cadmium and lead ions by biochar derived from date seeds in a packed column reactor. **Desalination and Water Treatment**, v. 250, p. 126-135, 2022.

SARMA, P. J. *et al*. Batch and Continuous Removal of Copper and Lead from Aqueous Solution using Cheaply Available Agricultural Waste Materials. **International Journal of Environmental Research**, v. 9, n. 2, 2015.

SAUDI, H. *et al*. Utilization of pure silica extracted from rice husk and FTIR structural analysis of the prepared glasses. **Semiconductors**, v. 24, p. 25, 2015.

SCHEUFELE, Fabiano Bisinella *et al*. Monolayer-multilayer adsorption phenomenological model: kinetics, equilibrium and thermodynamics. **Chemical Engineering Journal**, v. 284, p. 1328-1341, 2016.

SCHNEIDER, Lara Talita *et al*. Soybean hulls activated carbon for metronidazole adsorption: Thermochemical conditions optimization for tailored and enhanced meso/microporosity. **Journal of Analytical and Applied Pyrolysis**, v. 177, p. 106339, 2024.

SHANMUGAM, Devi *et al*. Bench-scale packed bed sorption of Cibacron blue F3GA using lucrative algal biomass. **Alexandria Engineering Journal**, v. 55, n. 3, p. 2995-3003, 2016.

SHEBL, Magdy *et al*. New non-toxic transition metal nanocomplexes and Zn complex-silica xerogel nanohybrid: Synthesis, spectral studies, antibacterial, and antitumor activities. **Journal of Molecular Structure**, v. 1118, p. 335-343, 2016.

SITHOLE, Thandiwe. A review on regeneration of adsorbent and recovery of metals: adsorbent disposal and regeneration mechanism. **South African Journal of Chemical Engineering**, v. 50, n. 1, p. 39-50, 2024.

SONG, Jiyun *et al*. Adsorption characteristics of methylene blue by peanut husk in batch and column modes. **Desalination**, v. 265, n. 1-3, p. 119-125, 2011.

STUMM, W. **Chemistry of the solid-water interface**. New York: Wiley, 1992. 448 p.

SULAYMON, Abbas H.; AHMED, Kawther W. Competitive adsorption of furfural and phenolic compounds onto activated carbon in fixed bed column. **Environmental Science & Technology**, v. 42, n. 2, p. 392-397, 2008.

SYUHADAH, Noor *et al*. Rice husk as biosorbent: a review. **Health Environ. J.**, v. 3, n. 1, p. 89-95, 2012.

TAHERI, E. S. *et al*. Investigation of hydrodynamic parameters in a novel expanded bed configuration: local axial dispersion characterization and an empirical correlation study. **Brazilian Journal of Chemical Engineering**, v. 29, p. 725-739, 2012.

TAKA, Anny Leudjo *et al.* Chitosan nanocomposites for water treatment by fixed-bed continuous flow column adsorption: A review. **Carbohydrate Polymers**, v. 255, p. 117398, 2021.

TATY-COSTODES, V. Christian *et al*. Removal of lead (II) ions from synthetic and real effluents using immobilized Pinus sylvestris sawdust: Adsorption on a fixed-bed column. **Journal of hazardous materials**, v. 123, n. 1-3, p. 135-144, 2005.

TCHOUNWOU, Paul B. *et al*. Heavy metal toxicity and the environment. Molecular, **Clinical and Environmental Toxicology: Volume 3: Environmental Toxicology**, p. 133-164, 2012.

THOMAS, Henry C. Heterogeneous ion exchange in a flowing system. **Journal of the American Chemical Society**, v. 66, n. 10, p. 1664-1666, 1944.

TSONEV, Tsonko; CEBOLA LIDON, Fernando Jose. Zinc in plants-an overview. **Emirates Journal of Food & Agriculture (EJFA)**, v. 24, n. 4, 2012.

VALVERDE, Abel; GRIFFITHS, Ian M. The role of adsorbent microstructure and its packing arrangement in optimising the performance of an adsorption column. **Discover Chemical Engineering**, v. 4, n. 1, p. 27, 2024.

VAREDA, João *et al*. Assessment of heavy metal pollution from anthropogenic activities and remediation strategies: a review. **Journal of Environmental Management**, v. 246, p. 101-118, 2019.

VÁZQUEZ, Gonzalo *et al.* Chestnut shell as heavy metal adsorbent: optimization study of lead, copper and zinc cations removal. **Journal of Hazardous Materials**, v. 172, n. 2-3, p. 1402-1414, 2009.

VEIT, Márcia Teresinha *et al.* Biosorption of nickel (II) ions by using chemically pre-treated Sargassum filipendula biomass in a fixed bed column. **World Journal of Microbiology and Biotechnology**, v. 25, n. 10, p. 1849-1856, 2009.

VIEIRA, M. G. A. *et al.* Adsorption of lead and copper ions from aqueous effluents on rice husk ash in a dynamic system. **Brazilian Journal of Chemical Engineering**, v. 31, p. 519-529, 2014.

VIOTTI, Paolo *et al*. Biochar as alternative material for heavy metal adsorption from groundwaters: lab-scale (column) experiment review. **Materials**, v. 17, n. 4, p. 809, 2024.

WANG, S. *et al*. Study on the synergistic co-pyrolysis behaviors of mixed rice husk and two types of seaweed by a combined TG-FTIR technique. **Journal of Analytical and Applied Pyrolysis**, v. 114, p. 109-118, 2015.

WANG, Wenqing *et al*. Adsorption of chromium (VI) by strong alkaline anion exchange fiber in a fixed-bed column: experiments and models fitting and evaluating. **Separation and Purification Technology**, v. 149, p. 16-23, 2015.

WANG, Xiangtao *et al.* Nanomaterials as sorbents to remove heavy metal ions in wastewater treatment. **J. Environ. Anal. Toxicol**, v. 2, n. 7, p. 154-158, 2012.

WANG, Yu *et al*. Guideline for modeling solid-liquid adsorption: kinetics, isotherm, fixed bed, and thermodynamics. **Chemosphere**, v. 349, 140736 p., 2024.

WILLIAMSON, Adam J. *et al*. Conjoint bioleaching and zinc recovery from an iron oxide mineral residue by a continuous electrodialysis system. **Hydrometallurgy**, v. 195, p. 105409, 2020.

WORLD HEALTH ORGANIZATION (WHO). **Guidelines for drinking-water quality**. 4ª ed. Geneva: WHO Press, 2011. 541 p.

XU, Zhe *et al*. Mathematically modeling fixed-bed adsorption in aqueous systems. **Journal of Zhejiang University SCIENCE A**, v. 14, n. 3, p. 155-176, 2013.

YAGUB, Mustafa T. *et al*. Fixed-bed dynamic column adsorption study of methylene blue (MB) onto pine cone. **Desalination and Water Treatment**, v. 55, n. 4, p. 1026-1039, 2015.

YAN, Guangyu *et al*., Min. A new model for heavy metal removal in a biosorption column. **Adsorption Science & Technology**, v. 19, n. 1, p. 25-43, 2001.

YOGESHWARAN, V.; PRIYA, A. K. Experimental studies on the removal of heavy metal ion concentration using sugarcane bagasse in batch adsorption process. **Desalination and Water Treatment**, v. 224, p. 256-272, 2021.

YOON, Young Hee; NELSON, James H. Application of gas adsorption kinetics I. A theoretical model for respirator cartridge service life. **American Industrial Hygiene Association Journal**, v. 45, n. 8, p. 509-516, 1984.

YU, Long Ying *et al*. Synthesis and characterization of silica by sol-gel method. **Advanced Materials Research**, v. 1030, p. 189-192, 2014.

YUN, Jun-Xian *et al*. Variation of the axial dispersion along the bed height for adsorbents with a density difference and a log-normal size distribution in an expanded bed. **Industrial & Engineering Chemistry Research**, v. 43, n. 25, p. 8066-8073, 2004.

YUNUS, Muhammad Arham. Extraction cellulose from rice husk. **Journal Akta Kimia Indonesia (Indonesia Chimica Acta)**, p. 79-83, 2019.

ZENG, Guangyong *et al.* Novel polyvinylidene fluoride nanofiltration membrane blended with functionalized halloysite nanotubes for dye and heavy metal ions removal. **Journal of Hazardous Materials**, v. 317, p. 60-72, 2016.

ZENG, Zhen *et al*. The model and mechanism of adsorptive technologies for wastewater containing fluoride: a review. **Chemosphere**, v. 340, p. 139808, 2023.

ZHANG, Ying *et al.* Characterization of H3PO4-treated rice husk adsorbent and adsorption of copper (II) from aqueous solution. **BioMed Research International**, v. 2014, n. 1, p. 496878, 2014.

ZHAO, Binglu *et al*. Adsorption of Congo red from solution using cationic surfactant modified wheat straw in column model**. Journal of Environmental Chemical Engineering**, v. 2, n. 1, p. 40-45, 2014.